

1 The changing mass of the Antarctic Ice Sheet during ENSO- 2 dominated periods in the GRACE era (2002-2022)

3 John Bright Ayabilah^{1,2}, Matt King^{1,2}, Danielle Udy², Tessa Vance³

5 ¹School of Geography, Planning, and Spatial Science, University of Tasmania, Hobart 7001, Tasmania, Australia

6 ²The Australian Centre for Excellence in Antarctic Science, Institute for Marine & Antarctic Studies, University
7 of Tasmania, Hobart 7001, Tasmania, Australia

8 ³Australian Antarctic Program Partnership, Institute for Marine & Antarctic Studies, University of Tasmania,
9 Hobart, TAS, 7001, Australia

10 *Correspondence to:* John Bright Ayabilah (johnbright.ayabilah@utas.edu.au)

13 **Abstract.** Large-scale modes of climate variability significantly influence Antarctic Ice Sheet (AIS) mass change.
14 Improved understanding of the relationship between these climate modes and AIS mass change can help reduce
15 uncertainties in future ice mass estimates and its contribution to sea level rise. However, the spatiotemporal
16 patterns of AIS mass variation driven by El Niño Southern Oscillation (ENSO)-induced atmospheric circulation
17 remain unclear. ~~Here, we investigated AIS mass variability during different ENSO periods using Gravity~~
18 ~~Recovery and Climate Experiment (GRACE) observed mass changes and modelled surface mass balance (using~~
19 ~~RACMO2.4p1)~~ over the period 2002 to 2022. ~~To allow comparison with GRACE, we used a cumulative sum~~
20 ~~indexing method to define different ENSO-dominated ‘periods’ over 2002-2022. This method results in time~~
21 ~~periods that are dominated by a particular phase of ENSO, that is not necessarily equivalent to specific events as~~
22 ~~derived from canonical indices.~~ The results show strong ~~event to event~~ spatial variability in how the ENSO
23 teleconnection ~~cumulatively~~ manifests over the AIS. These differing spatial patterns are primarily driven by
24 changes in the Amundsen Sea Low (~~ASL~~) strength, location, and extent, which alter circulation patterns and
25 moisture flow in West Antarctica. In East Antarctica, ice mass variability is largely influenced by the positioning
26 of cyclonic and anticyclonic ~~circulation~~ anomalies, primarily driven by the Southern Annular Mode (~~SAM~~);
27 however, ENSO signals are also present. In both East and West Antarctica, this study shows that the spatial impact
28 of any given ENSO-dominant period event, as derived using standard tropical atmospheric metrics (Sea Surface
29 Temperature (SST) and pressure anomalies), and its influence on the ASL and Southern Ocean circulation can be
30 equally (and in some cases more) important to AIS variability can trigger distinct circulation patterns which can
31 variably influence surface mass balance and ice mass change. However, uncertainties remain, as the mass
32 variability observed during ENSO-dominant periods may not be solely attributed to ENSO, due to teleconnections
33 that may not have fully developed or may have been masked by other processes. GRACE provides an opportunity
34 to understand event scale ENSO precipitation independently of numerical models.

35 1. Introduction

36 The drivers of inter-annual to decadal Antarctic Ice Sheet (AIS) mass variability are complex and not yet fully
37 understood (IMBIE Team, 2018). External factors, such as episodic extreme precipitation events often linked to
38 atmospheric rivers (Wille et al., 2021), and internal factors, including ice dynamics (IMBIE Team, 2018), both

39 contribute to these variations. Understanding the mechanisms underlying AIS mass change and variability is
40 critical for improving future projections of ice mass changes and the Antarctic contribution to sea level rise.

41 The main determinants of the net AIS mass balance (MB) are ice discharge (D) from the continental margins of
42 Antarctica and Surface Mass Balance (SMB). SMB is further defined as accumulating precipitation and riming
43 onto the ice sheet, minus runoff, sublimation/evaporation and blowing snow erosion. The fluctuation of the AIS
44 mass balance and its subsequent contribution to sea level rise are based on the difference between ice discharge
45 and SMB (i.e., $MB = SMB - D$). The AIS SMB exhibits high variability on inter-annual to decadal timescales,
46 (Kim et al., 2020; Medley and Thomas, 2019; Van De Berg et al., 2006). Precipitation variability, driven by
47 atmospheric circulation, is a key determinant of Antarctic SMB and, over a wide range of timescales, including
48 interannual to decadal, is closely linked to modes of climate variability (Kim et al., 2020).

49 The Southern Annular Mode (SAM) is the dominant mode of extratropical variability in the Southern Hemisphere.
50 The SAM signal is driven by a combination of internal atmospheric dynamics and external forcings, including
51 stratospheric ozone depletion, increases in greenhouse gases, and tropical teleconnections (Fogt and Marshall,
52 2020b). It varies on timescales from weeks to decades, and its influence on Antarctic precipitation is regionally
53 dependent and affects different regions of Antarctica in distinct ways (Marshall et al., 2017). During the positive
54 phase of SAM, the westerlies around 60° S strengthen, and the overall impact on the AIS is a net decrease in
55 SMBmid-latitude westerly wind belt contracts poleward, with a reduction in net precipitation across Antarctica
56 (Marshall et al., 2017; Medley and Thomas, 2019). Conversely, the net influence of the negative phase of SAM
57 on the AIS is an increase in SMB, is associated with increased net precipitation over the continent (Medley and
58 Thomas, 2019; Marshall et al., 2017). Regionally, the contraction of the storm track during positive SAM
59 strengthens the westerlies around 60° S, enhancing moisture transport to the coastal regions of West Antarctica
60 and the western Antarctic Peninsula, which increases precipitation. In contrast, the contraction of the westerlies
61 reduce moisture transport to the interior of East Antarctica, decreasing precipitation, with the reverse pattern
62 occurring during negative SAM (Medley and Thomas, 2019; Marshall et al., 2017). However, SAM related
63 circulation patterns are not stationary and vary over decades, meaning the regional impacts may shift over time
64 (Marshall et al., 2013).

65 The El Niño Southern Oscillation (ENSO) is the dominant mode of inter-annual climate variability globally (2–
66 7-year timescales) and is defined by variations in sea surface temperature (SST) anomalies in the tropical Pacific
67 (McPhaden et al., 2006). The ENSO pathway to Antarctica is modulated by the Amundsen Sea Low (ASL)
68 which lies at the poleward end of the Rossby wave train originating in the tropics (Hoskins and Karoly, 1981).
69 This Rossby wave train leads to the formation of the Pacific South American mode 1(PSA-1), an atmospheric
70 anomaly pattern that enables ENSO signals to reach Antarctica (Hoskins and Karoly, 1981). These
71 interactions This creates a high positive pressure anomaly over the Amundsen-Bellingshausen sector (ABS)
72 during El Niño events the positive phase of PSA-1 and low negative pressure anomaly during La Niña
73 conditions the negative phase of PSA-1 (Turner, 2004; Hoskins and Karoly, 1981). The ASL represents a
74 climatological area of low pressure in the South Pacific and is a key component of the nonzonal climatological
75 circulation (Raphael et al., 2016b). The teleconnection between ENSO and the ASL is strongest during the austral
76 spring (September-November; SON) but exerts influence throughout the year (Schneider et al., 2012; Clem and

77 Fogt, 2013; Fogt et al., 2011). The strength, extent, and location of the ASL shows significant variability during
78 different ENSO phases and individual ENSO events, resulting in varying atmospheric circulation patterns that
79 strongly influences moisture and temperature distribution in West Antarctica (Raphael et al., 2016b; Hosking et
80 al., 2013). ~~The impact of ENSO on East Antarctica through the ASL is not fully clear (Zhang et al., 2021; King
81 et al., 2023).~~

82 The impact of ENSO on Antarctic climate is modulated by the phase of SAM, with the signal amplified when
83 SAM and ENSO are atmospherically in phase (positive SAM/La Niña or negative SAM/El Niño) and reduced
84 when they are atmospherically out of phase (positive SAM/El Niño or negative SAM/La Niña) (Clem et al., 2016;
85 Fogt et al., 2011). Positive SAM and La Niña conditions are associated with a deepening (i.e. lower pressure
86 anomaly) ASL, while negative SAM and El Niño conditions weaken the ASL, and influence its longitudinal shift
87 (Raphael et al., 2016b; Hosking et al., 2013). The deepening of the ASL induces continental wind outflow on its
88 western flank, reducing precipitation and SMB ~~over the Antarctic Peninsula and from the Bellingshausen Sea to
89 the Ross Sea region~~ in West Antarctica, whereas a weakened ASL leads to onshore winds that enhance
90 precipitation and SMB (Zhang et al., 2021; Li et al., 2022a). The longitudinal shift of the ASL modifies these
91 impact zones.

92 The spatial patterns and magnitude of AIS mass variability due to large-scale modes of climate variability remain
93 unclear. Studies on the role of ENSO in Antarctic climate have mostly focused on precipitation derived from
94 reanalysis products or modelled SMB data (e.g., Medley and Thomas, 2019; Clem et al., 2016; Clem and Fogt,
95 2013; Fogt et al., 2011). Only a few studies have examined the relationship between large-scale modes of climate
96 variability and recent observed ice mass variation using Gravity Recovery and Climate Experiment (GRACE)
97 observed AIS ice mass change time series on timescales ranging from months to decades (e.g., Bodart and
98 Bingham, 2019; Zhang et al., 2021; King et al., 2023). Most of these studies have focused on single strong ENSO
99 events, such as the 2015-2016 El Niño (Bodart and Bingham, 2019), or on the mean impact of ENSO on the AIS.
100 ~~In contrast, our study investigates the spatial impacts of multiple individual ENSO periods (as defined in our
101 study), enabling an assessment of how AIS mass variability differs between events and capturing the diverse
102 responses across the ice sheet, rather than a mean response.~~

103 The GRACE mission, launched in 2002, has contributed to our understanding of the redistribution of mass within
104 the Earth system, which is useful for observing changes of the Greenland and Antarctic ice sheets (Tapley et al.,
105 2004; Shepherd et al., 2012). GRACE-observed ice mass variability is related to atmospheric circulation-driven
106 snow accumulation and variation in ice discharge (Diener et al., 2021). ~~Although mass loss from runoff and
107 sublimation is included in the GRACE signal, these components are relatively minor compared to discharge. Over
108 the interannual timescales, with atmospheric variability dominates the observed mass changes over interannual
109 timescales~~ (King et al. 2023). Studies of ENSO's impact on AIS using GRACE-observed ice mass changes show
110 that different ENSO events result in varying climatic and surface weather effects, leading to different spatial
111 patterns of AIS mass variability. Bodart and Bingham (2019) demonstrated that during the 2015-2016 El Niño,
112 the Antarctic Peninsula and West Antarctica gained mass, while East Antarctica experienced a reduction in mass.
113 This spatial pattern is also consistent over a longer period, in line with Zhang et al. (2021) who found similar
114 correlations. They observed a bipolar spatial pattern: during El Niño events, there was a mass gain over the

115 Antarctic Peninsula and West Antarctica and a mass loss over East Antarctica, while the pattern reversed during
116 La Niña events. The bipolar spatial patterns are consistent with the results of King et al. (2023), based on a GRACE
117 analysis for the period 2002-2021, and King and Christoffersen (2024), which used GRACE and altimetry data
118 (2002-2020), despite differences in approaches and study periods. However, other studies have suggested that
119 specific ENSO events and types of ENSO events have distinct impacts on Antarctic SMB that are not limited to
120 a bipolar pattern (e.g., Macha et al., 2024; Sasgen et al., 2010).

121 This study aims to investigate the spatial patterns of ice mass change and the driving atmospheric circulation
122 conditions during various ENSO-dominated periods, as observed in GRACE-derived AIS mass variations
123 between 2002 and 2022. Since GRACE observes total mass change without distinguishing between the individual
124 components of the mass balance, we use SMB output from a regional climate model RACMO2.4p1 to assess the
125 contribution of SMB to the spatial patterns detected by GRACE. The results indicate that no two ENSO
126 periods~~events~~ have the same net effect on Antarctic ice mass, especially at regional scales, and the bipolar spatial
127 pattern observed in earlier studies is not consistent across all ENSO events. This variability suggests that the
128 ENSO signal in the AIS is shifted from its background pattern depending on event-specific atmospheric and
129 oceanic factors.

130 **2. Data and Methods**

131 **2.1. AIS mass change**

132 We used the GRACE and GRACE Follow On data. The data are provided by the GFZ German Research Centre
133 for Geosciences (Landerer et al., 2020). The GRACE Follow-On mission, launched in May 2018, succeeded the
134 GRACE mission, which was decommissioned in October 2017 due to battery and fuel problems. This gap between
135 the GRACE and GRACE Follow-On missions resulted in the loss of data from July 2017 and May 2018. Our
136 analysis involved GRACE data spanning from April 2002 to Dec 2022 without gap filling. We used the COST-G
137 release 1 version 3 (RL-01 V0003) gridded mass anomaly product, which combines GRACE/GRACE-FO
138 solutions from multiple GRACE analysis centres (Landerer et al., 2020). The data are provided on a -50 km
139 gridded products with approximately monthly temporal sampling. However, but note that GRACE data have an
140 underlying spatial resolution of ~300km (Sasgen et al., 2020; Dahle et al., 2024). This relatively coarse resolution
141 limits GRACE's ability to resolve or capture relatively small mass changes, particularly those associated with
142 localised SMB anomalies.

143 The various available GRACE data products differ based on the processing methods and background models used.
144 The gridded mass change product adopted here is initially derived by solving for spherical harmonic coefficients
145 and then computing mass anomalies for each grid cell across the entire ice sheet using tailored sensitivity kernels
146 that minimise both GRACE and leakage error (Groh and Horwath, 2016). Within this product, glacial isostatic
147 adjustment is corrected using the ICE6G_D model (Richard Peltier et al., 2018), although this has no bearing on
148 non-linear variability as studied here. Atmospheric and oceanic effects on mass redistribution are also modelled
149 as are spherical harmonic degree-1 terms based on the approach of Swenson et al. (2008). Further details about
150 the GRACE time series, post-processing techniques, and quality assessment can be found in Dahle et al. (2019).
151 It is worth noting that the GRACE-observed ice mass change time series is affected by systematic errors associated

152 with the GRACE orbital geometry and small unmodelled errors, evident in the (largely north-south) striping
153 pattern observed in some of the ice mass change results.

154 We focus our analysis on the ENSO signal in ice mass variation during different ENSO-dominated periods. First,
155 we removed short-term signal fluctuations in the GRACE data by applying a 7-month moving median smoother
156 to the GRACE time series. This filter choice, following King et al. (2023), is a subjective decision aimed at
157 dampening month-to-month noise without distorting longer-term variability. Since our focus is on GRACE-
158 observed ice mass variability, we subtracted the linear trend at each grid point, estimated using ordinary least
159 squares over the data span. This effectively produces mass anomalies with respect to the climatology of the entire
160 GRACE period.

161 To understand the relationship between ice mass changes and ENSO-dominated periods, we computed the rate of
162 ice mass change for each identified ENSO-dominated period. These rates represent the impact of ENSO during
163 each ENSO-dominated period. We calculated the rates for each grid cell of the gridded GRACE ice mass anomaly
164 data and generated spatial patterns of ice mass trends for each ENSO-dominated period.

165 **2.2. Climate indices**

166 To characterise ENSO variability, we used the Niño3.4 index, one of several metrics that measures the strength
167 and phase of ENSO based on sea surface temperature anomalies in the central and eastern tropical Pacific. This
168 index is obtained by tracking the running five-month mean SST based on the HadISST record over 5°N–5°S,
169 170°W–120°W (Rayner et al., 2003) and is normalised and shown in Fig. 1a. It is provided by the Climate
170 Prediction Centre (CPC) of the National Oceanic and Atmospheric Administration (NOAA) and can be accessed
171 at <https://psl.noaa.gov/data/timeseries/month/Nino34/>. The Niño3.4 temperature anomalies are standard for
172 detecting and monitoring ENSO events but cannot differentiate between eastern and central ENSO events. We
173 used the Niño3.4 index because our focus was on the spatial variability in AIS mass during all ENSO events,
174 rather than differentiating between eastern and central ENSO events.

175 For SAM, we used the station-derived index from Marshall (2003), available at [http://www.nerc-
176 bas.ac.uk/icd/gjma/sam.html](http://www.nerc-bas.ac.uk/icd/gjma/sam.html), and shown in Fig. 1a. This index is based on the zonal pressure differences at 12
177 stations located between 40 °S and 65 °S.

178 To identify ENSO signatures in the GRACE data, we first identified El Niño- and La Niña-dominated periods
179 based on the cumulative summed indices, which act as a sort of low-pass filter of the raw indices. The cumulative
180 summed indices were derived from anomalies relative to their climatological mean using a reference window of
181 1971-1999. This period is a well observed period before the commencement of GRACE and is the same as that
182 chosen by King et al. (2023). After the indices were normalised using the mean and standard deviation computed
183 within the reference window, the normalised indices were restricted to the GRACE period, cumulatively summed,
184 detrended, and renormalised.

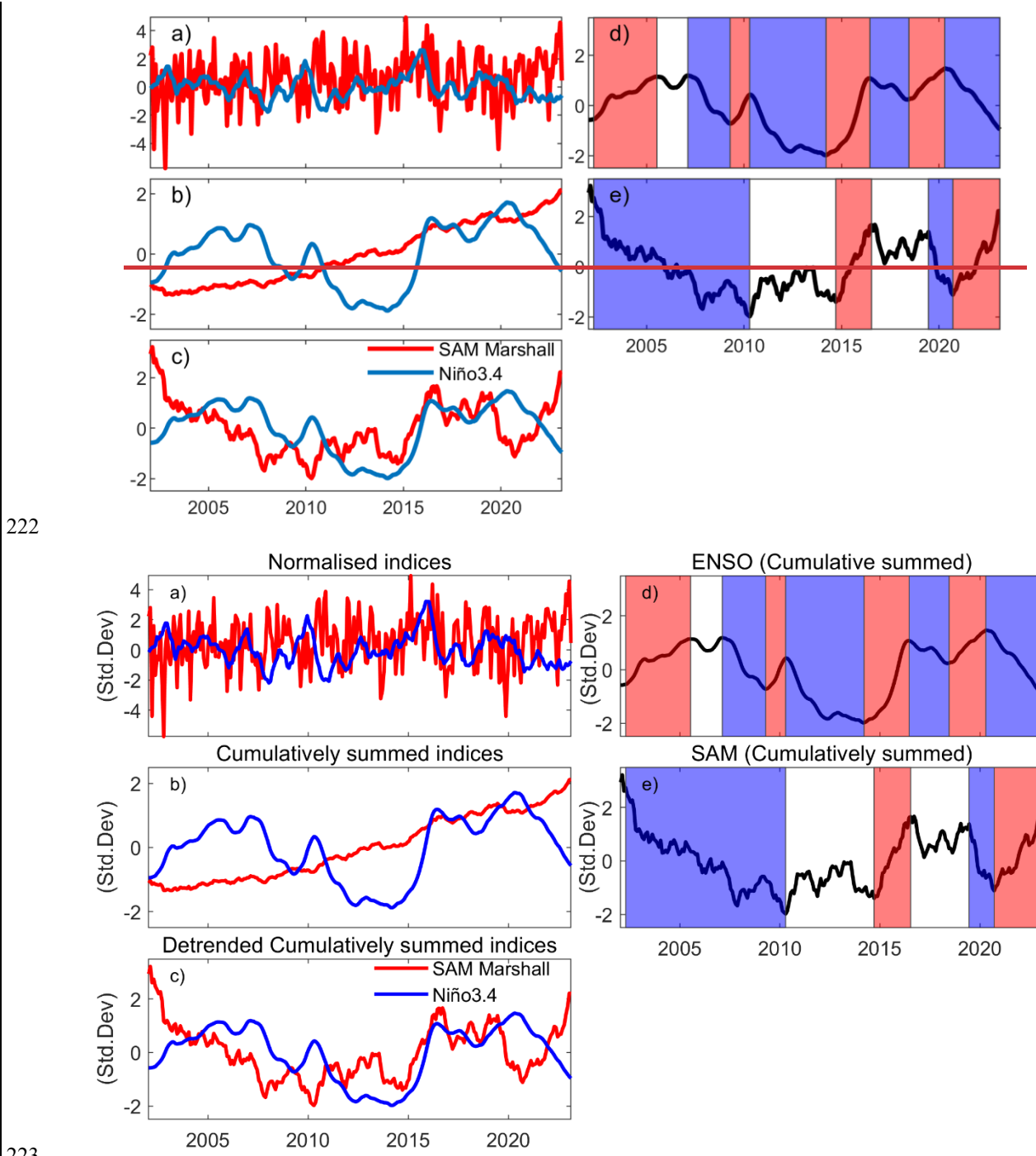
185 To investigate the potential linkage between large-scale climate variability and ice mass variation, we
186 cumulatively summed all the climate indices as shown in (Fig 1b) and detrended (Fig. 1c). The AIS mass reflects
187 the compound effect of surface mass fluxes over time. The cumulative mass flux observed by GRACE reflects

188 the cumulative climate indices (King et al., 2023) as opposed to raw indices, which relate to mass flux. These
189 cumulative indices are also captured by modelled cumulative SMB (Kim et al., 2020; Diener et al., 2021). The
190 alternative approach is to difference GRACE data in time, but this inflates the GRACE noise and reduces the
191 lower frequency signal and is hence undesirable (King et al., 2023).

192 ~~To identify ENSO signatures in the GRACE data, we first identified El Niño and La Niña dominated periods~~
193 ~~based on the cumulative summed indices, which essentially act as a low pass filter of the raw indices. The~~
194 ~~cumulative summed indices were derived from anomalies relative to their climatological mean using a reference~~
195 ~~window of 1971–2000. This period is a well observed period before the commencement of GRACE and is the~~
196 ~~same as that chosen by King et al. (2023). After the indices were normalised using the mean and standard deviation~~
197 ~~computed within the reference window, the normalised indices were restricted to the GRACE period, cumulatively~~
198 ~~summed, detrended, and renormalised.~~

199 In this study, we defined El Niño-dominated periods as ~~intervals during which the positive phase of ENSO persists~~
200 ~~and outweighs the negative phase, culminating in a positive peak in the cumulative ENSO index. those where the~~
201 ~~positive phase of ENSO dominates the negative ENSO phase until a positive peak in the cumulative index is~~
202 ~~reached. Conversely~~Similarly, La Niña-dominated periods are defined as ~~intervals during which negative phase~~
203 ~~outweighs the positive phase, culminating in a negative peak those in which the negative phase dominates until a~~
204 ~~negative peak is reached. Only ENSO periods with a minimum duration of 12 months were considered in our~~
205 ~~analysis.~~ In a cumulatively summed index, these are expressed as sustained periods of positive (El Niño) or
206 negative (La Niña) slope. Based on this criterion, we identified four El Niño-dominated periods over the GRACE
207 time steps: 2002–2005, 2009–2010, 2014–2016, and 2018–2020 (Fig. 1d). An equal number of La Niña-dominated
208 periods were found, covering 2007–2009, 2010–2014, 2016–2018, and 2020–2022. The strength of the expression
209 of the ENSO signal in the Antarctic climate is modulated by the phase of SAM (Fogt et al., 2011). During the
210 2002–2005 El Niño-dominated period, the cumulative SAM index was dominated by negative SAM until around
211 2008 (atmospherically in phase El Niño/-SAM). After 2008, the cumulative SAM index exhibited no notable
212 trend, indicating a neutral phase. During the 2014–2016 El Niño, cumulative SAM and ENSO indices were
213 atmospherically out of phase (El Niño/+SAM). SAM shifted to a neutral state during the 2016–2018 La Niña.
214 SAM and ENSO were atmospherically in phase during the 2018–2020 El Niño (El Niño/-SAM) and 2020–2022
215 La Niña (La Niña/+SAM), which is notable as the only time positive SAM and La Niña co-occurred over the
216 GRACE period (Fig. 1d, e).

217 Note that we do not distinguish between Central Pacific (CP) and Eastern Pacific (EP) El Niño events in our
218 analysis because our ENSO dominated periods frequently span multiple years. Indeed, examining the cumulative
219 CP and EP indices shows they are very similar, aside from 2016–2018, and hard to distinguish in an analysis of
220 GRACE data (Supplementary Fig. S1). Our method using the Nino3.4 index encapsulates variations in the tropical
221 spatial pattern of SST anomalies.



233 ~~are reached in the cumulatively summed SAM index (Marshall, 2003) are defined as SAM-positive and~~
234 ~~SAM-negative dominated periods, respectively, denoted as red and blue shaded areas in (e) represent~~
235 ~~SAM positive and SAM negative dominated periods. Neutral dominated periods are represented by white~~
236 ~~shading.~~

237 2.3. SMB model outputs

238 We used modelled SMB output from the Regional Atmospheric Climate Model RACMO2.~~43p21~~ model (Van
239 Wessem, 2023; Van Dalum et al., 2025; Van Dalum et al., 2024). This model has a horizontal resolution of ~~2711~~
240 km and a vertical resolution of 40 atmospheric levels. This version of SMB model output is forced by ERA5
241 reanalysis data at its lateral ~~and ocean~~ boundaries ~~and SST and sea ice extent at the sea surface boundary~~, with
242 data available from 1979 onward. ~~Compared with previous releases, RACMO2.4p1 provides a better~~
243 ~~representation of SMB process which agree with observation (Van Dalum et al., 2025; Van Dalum et al., 2024).~~
244 For our study, monthly SMB values truncated to the GRACE period were used, covering Apr 2002 to Dec 2022.
245 To compare with GRACE data, we computed anomalies relative to the 2002-2022 mean and then cumulatively
246 summed them to obtain cumulative SMB anomalies in units of kg m^{-2} . These anomalies were then interpolated to
247 match the GRACE grid spacing and time steps. We detrended the cumulative SMB and performed a regression
248 analysis on these anomalies for each defined ENSO-dominated period.

249 2.4. Reanalysis climate data

250 To explore the potential climatic forcing during an ENSO-dominated period, we examined monthly mean ERA5
251 reanalysis model 10 m winds and sea level pressure from 2002 to 2022, with a resolution of 0.25° by 0.25°
252 (Hersbach et al., 2020). Anomalies of 10 m zonal and meridional wind components, as well as sea level pressure,
253 were computed for each grid cell relative to the mean over the GRACE period, for all regions south of 40° S. We
254 then computed anomaly composite means for each ENSO-dominated period. ~~We used ERA5 products instead of~~
255 ~~RACMO outputs because ERA5 provides broader spatial coverage and is more suitable for capturing large-scale~~
256 ~~atmospheric circulation patterns, which are critical for analysing ENSO-related teleconnections. Additionally,~~
257 ~~RACMO is forced by ERA5.~~

258 2.5. Definitions of events, periods and anomaly interpretations used in this study

259 We acknowledge that we use multiple terminologies in this study to define both our results, and when comparing
260 to the literature. For example, we use the term ‘El Niño- or La Niña-dominated period’ ~~or simply ‘period’~~ to define
261 the periods of time ~~of sustained ENSO phase~~ we define using our cumulatively summed index. In contrast, when
262 comparing to or describing other literature, we use the term ‘El Niño/ La Niña event’ which refers to the peak
263 phase of ENSO events. We also describe anomalies from the mean over the GRACE period. For the purposes of
264 this study, the pressure and wind fields, as well as SMB and GRACE mass change, depicted in the figures
265 represent anomalies from the climatology for each relevant variable. That is, for a given wind and pressure map,
266 the fields depict wind and pressure anomalies against the 2002-2022 mean (the GRACE data period). ~~For~~
267 ~~example~~~~Specifically~~, positive anomalies over the Antarctic continent reflect a ~~relative~~ strengthening of the mean
268 Antarctic ~~h~~High-pressure system, while negative anomalies reflect a ~~relative~~ weakening of the ~~Antarctic~~ ~~h~~High

269 pressure (not the presence of a low pressure system). SimilarlyFor SMB, positive SMB and GRACE anomalies
270 represent an increase in mass, whereas negative anomalies indicate a reduction in mass relative to the climatology.

271 2.6. Statistical significance of the results

272 To quantify the significance of our regression trends at each grid point, we employed a two-tailed Student's t-test.
273 The standard error of the slope at each grid point was calculated from the regression residuals and used to assess
274 whether the slope significantly differed from zero at the 5% significance level. For mean sea level pressure
275 anomaly composites, statistical significance was assessed based on deviations from the climatological baseline
276 using a two-sample t-test assuming unequal variances, also at the 5% significance level.

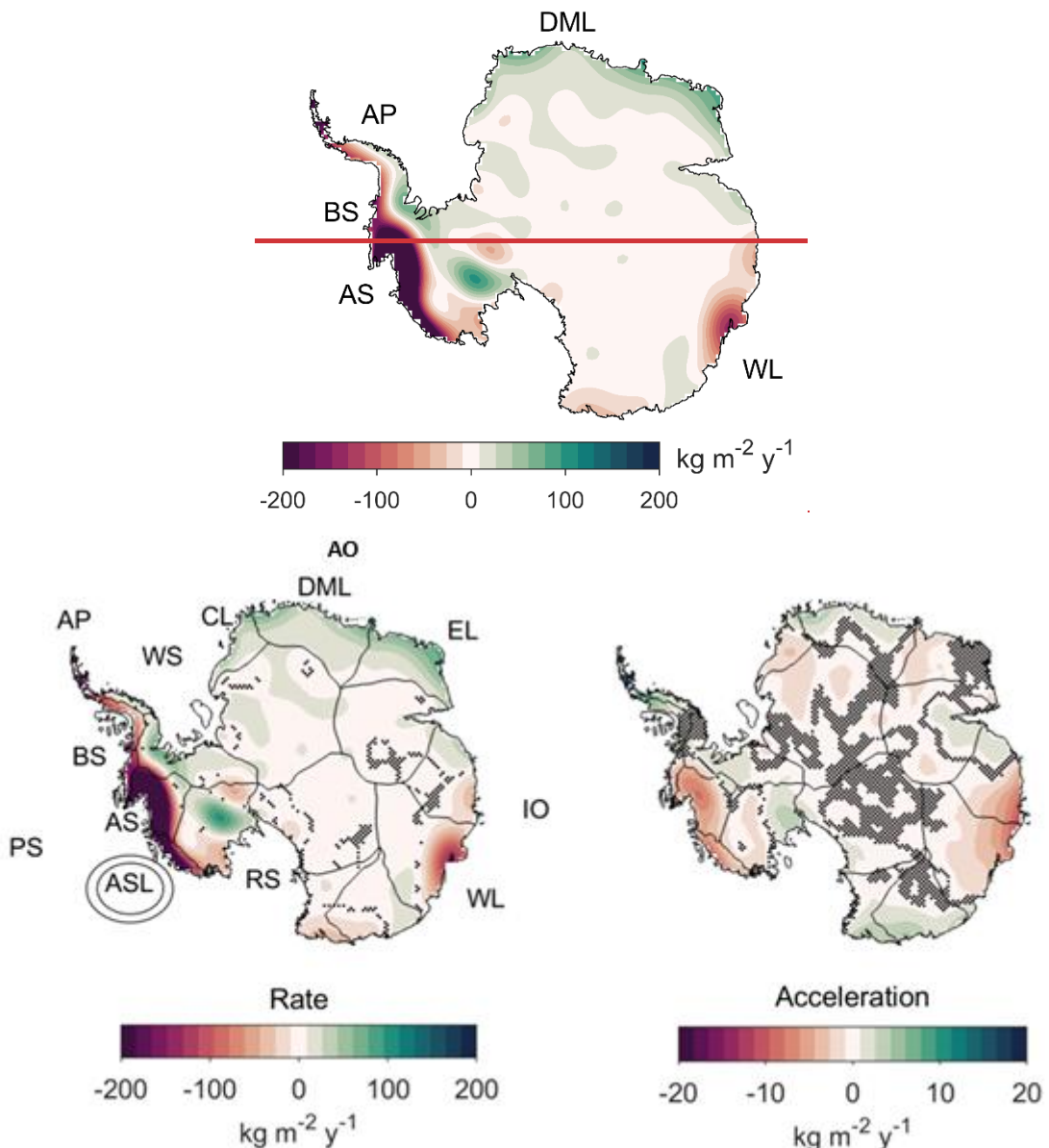
277 **3. Results**

278 **3.1 Ice mass change**

279 We start by examining the long-term trend and acceleration in AIS mass change over the GRACE observational
280 period, represented by the linear and quadratic terms in the regression, respectively (Fig. 2). The spatial pattern
281 reveals strong regional variability, with areas of both positive and negative mass anomalies. While not identical,
282 the linear rate and acceleration exhibit closely aligned spatial patterns of mass change. In West Antarctica, the
283 rate of ice mass loss is most pronounced in the Amundsen SeaEmbayment and Bellingshausen Sea sectors, where
284 accelerated ice discharge is well documented (Rignot et al., 2019; Gardner et al., 2018). The East Antarctic ice
285 sheet shows mass gain across Dronning Maud Land (and through to Enderby Land); conversely, whereas the
286 Wilkes Land sectorion has experienced a decline in mass. The negative acceleration observed in the Amundsen
287 Sea sector and Wilkes Land indicates that the rate of mass loss in these regions is increasing over time.

288 While the long-term trend in AIS mass is primarily driven by ice dynamics, the interannual variability is more
289 closely linked to changes in precipitation (Kim et al., 2020). Short-term mass fluctuations can be influenced by
290 large-scle circulation modes. To explore the impact of ENSO on ice mass variability, we next examine how
291 atmospheric circulation and mass anomalies respond to ENSO forcing.

292



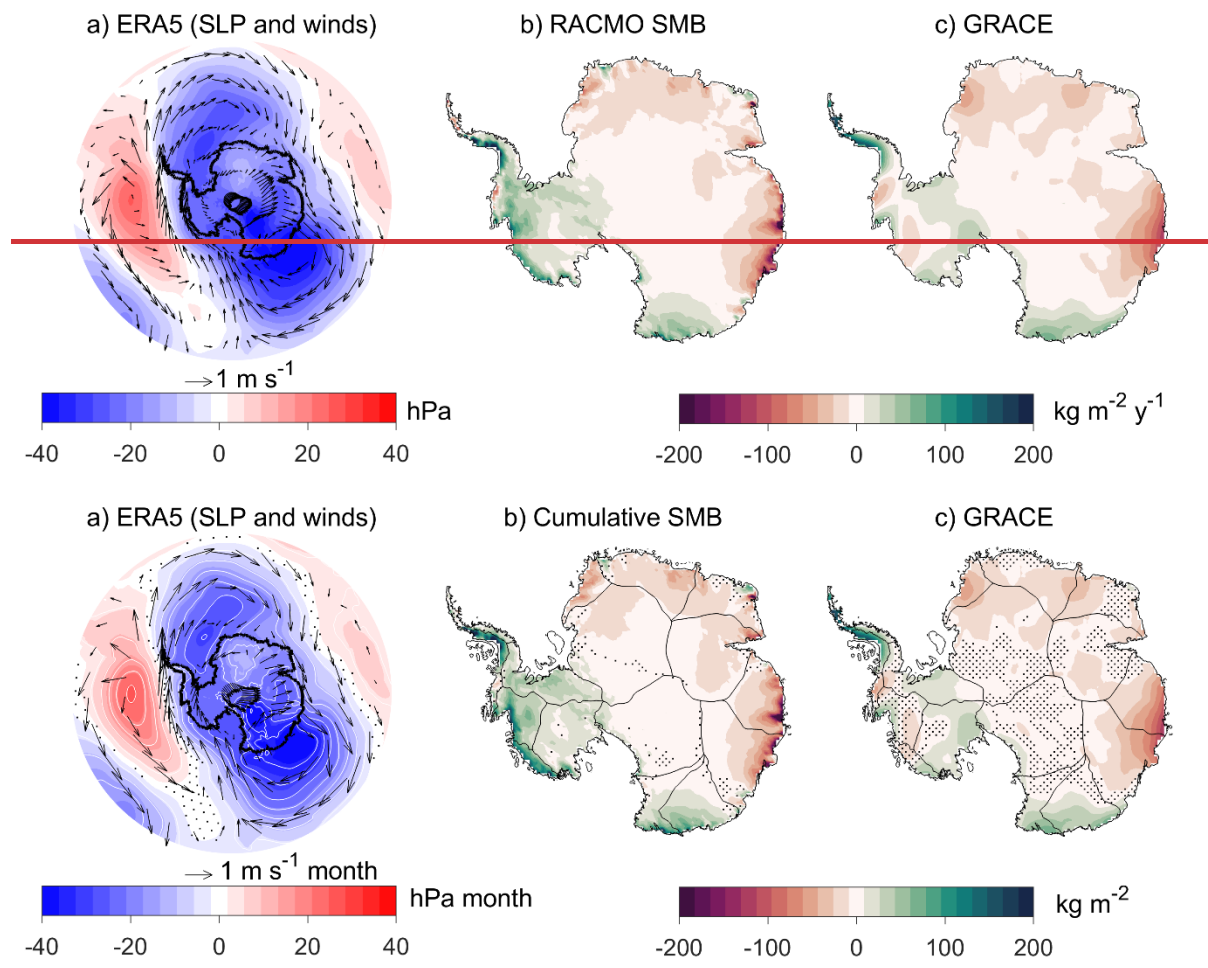
293

294 **Figure 2. AIS-H linear rate and acceleration of AIS trend in ice mass change (2002-2022) based on**
 295 **GRACE data from using univariate regression. Key Antarctic regions are labelled of interest are**
 296 **highlighted: Antarctic Peninsula (AP), Bellingshausen Sea (BS), Amundsen Sea (AS), Amundsen Sea Low**
 297 **(ASL), Pacific Sector (PS), Ross Sea (RS), Indian Ocean (IO), Atlantic Ocean (AO), Wilkes Land (WL),**
 298 **Enderby Land (EL), and Dronning Maud Land (DML), Coats Land (CL), and Weddell Sea (WS).**
 299 **Stippling indicates areas not statistically significant ($p < 0.05$). Significance tests do not reflect the effects of**
 300 **temporal correlations in these data (Williams et al., 2014).**

301

302 Figure 3 presents the regression results of cumulatively summed anomalies in ERA5 reanalysis climate variables
 303 (sea level pressure and 10 m winds) and RACMO2.4p1 model SMB, along with GRACE-derived ice mass change

304 anomalies, against the cumulatively summed Niño3.4 index. All variables were detrended before regression to
 305 focus on the variability. The results show that the cumulative ENSO is associated with shifts in influences
 306 atmospheric circulation that supports the observed dipole SMB and ice mass anomaly between over West and East
 307 Antarctica (Fig. 3a), driving short term fluctuation in AIS mass around the overall trend. ENSO induced changes
 308 in meridional flow regulate precipitation patterns, making SMB a primary driver of AIS mass variability. Since
 309 SMB directly influences ice mass changes, this results in spatially coherent patterns between SMB and GRACE-
 310 derived ice mass change (Fig. 3b–c). A substantial portion of the ENSO and SAM signals in GRACE observed
 311 ice changes can be linked to SMB variability (Kim et al., 2020; King et al., 2023).



314 **Figure 3.** Maps show the regression of terms for cumulatively summed sea level pressure (shaded
 315 region and contour) and 10 m wind anomalies (represented by reference vectors (m s⁻¹) from ERA5
 316 reanalysis (a), cumulatively summed RACMO2.4p1 model SMB anomalies (b), and GRACE ice mass
 317 change anomalies (c) when regressed against cumulatively summed Niño3.4. The u and v wind
 318 components were regressed separately. All panels reflect regression anomalies over the period 2002–2022.

319 All variables are linearly detrended prior to regression using the full data periods. Stippling
 320 indicates regions where the regression results are not statistically significant ($p < 0.05$).

322 The positive SMB anomalies in West Antarctica and negative anomalies in East Antarctica align with findings
323 indicating increased precipitation during El Niño and reduced precipitation during La Niña (Zhang et al., 2021;
324 Zhan et al., 2021). During El Niño events, strengthened onshore winds over West Antarctica enhance SMB, while
325 intensified offshore winds over East Antarctica reduce SMB. Conversely, during La Niña events, the circulation
326 pattern reverses, with increased moisture transport into East Antarctica and reduced onshore winds over West
327 Antarctica. As a result, SMB increases in East Antarctica while decreasing in West Antarctica. In West Antarctica,
328 the SMB signal differs from GRACE derived ice mass changes, whereas in East Antarctica, the two signals are
329 more closely aligned. This suggests that SMB variability is the primary driver of ice mass changes in East
330 Antarctica but not necessarily in West Antarctica. The discrepancy may stem from the near instantaneous
331 response of ice dynamics to ENSO driven oceanic forcing and/or mismodelled SMB (IMBIE Team, 2018; Rignot
332 et al., 2019), with the latter being more likely (King and Christoffersen, 2024).

333 We also compared the regression results presented in Figure 3 with El Niño and La Niña composites (see
334 supplementary Fig. S2) derived from annual accumulated SMB anomalies and annual mean Niño3.4 index, which
335 broadly agree with the cumulative approach spatial patterns observed in West and East Antarctica. From the
336 composite map (supplementary Fig. S2 covering 2002-2022), we observe that in West Antarctica, El Niño years
337 are associated with a positive mean SMB anomaly ($26.98 \text{ kg m}^{-2} \text{ yr}^{-1}$), while La Niña years correspond to a
338 negative mean anomaly ($-10.29 \text{ kg m}^{-2} \text{ yr}^{-1}$). In contrast, East Antarctica shows a negative mean SMB anomaly
339 ($-3.14 \text{ kg m}^{-2} \text{ yr}^{-1}$) during El Niño years and a positive anomaly ($5.28 \text{ kg m}^{-2} \text{ yr}^{-1}$) during La Niña years.

340 Our result shows that, spatially, SMB and ice mass increases in West Antarctica and decrease in East Antarctica
341 during El Niño-dominated periods, with the pattern reversing during La Niña-dominated periods (Fig. 3b, c). The
342 cumulative ENSO-induced changes in meridional flow are associated with the SMB variability (Fig. 3a, b). Since
343 changes in SMB are closely linked to ice mass change, the spatially coherent patterns between SMB and GRACE-
344 derived ice mass change (Fig. 3b–c).

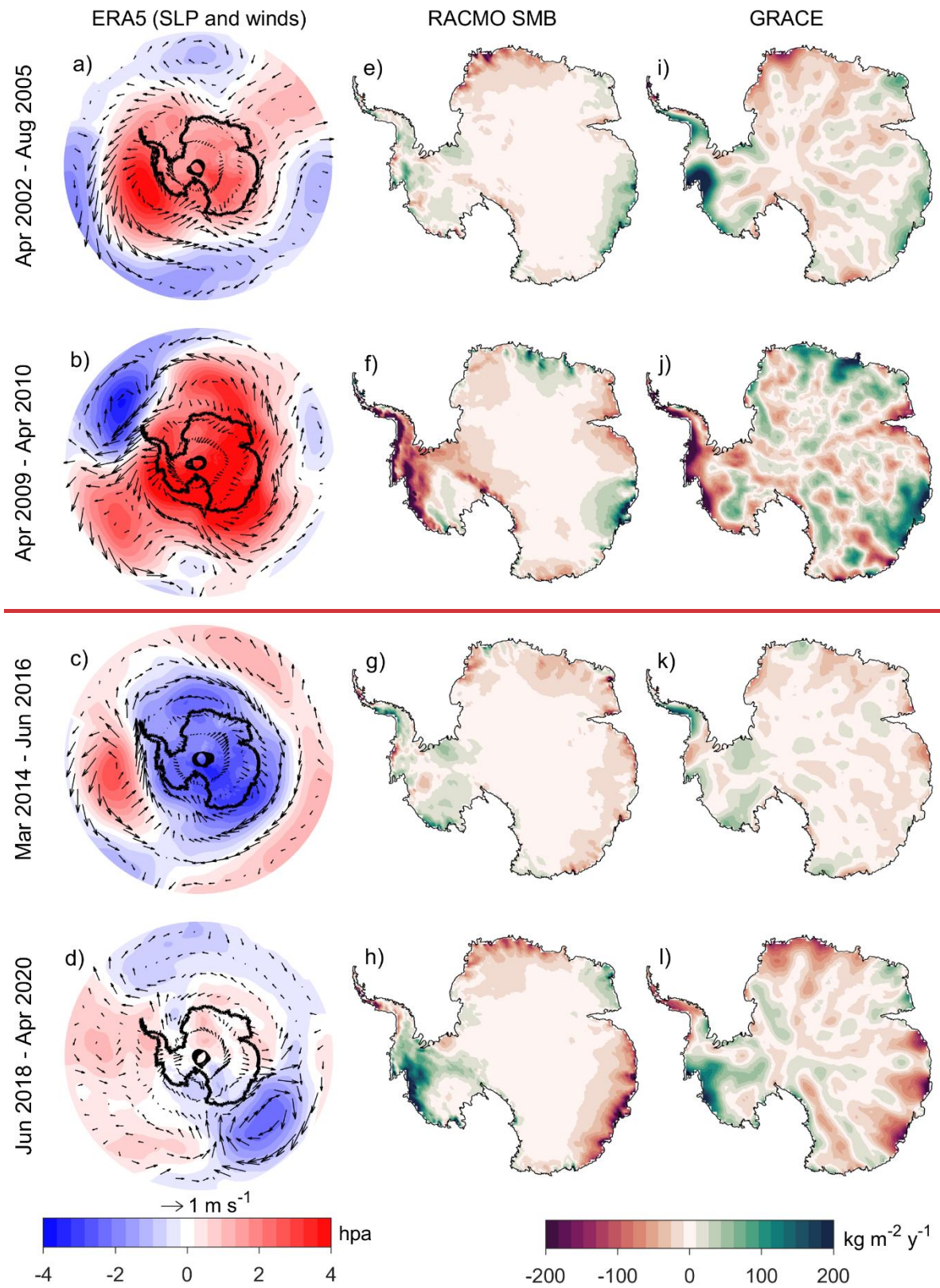
345 However, in West Antarctica, the SMB signal differs from GRACE-derived ice mass changes, which indicate
346 relatively modest positive mass anomalies compared to the stronger SMB signal (Fig. 3b, c), whereas in East
347 Antarctica, the two signals are more closely aligned.

348 We next focus on the variability within ENSO-dominated periods and find Given that no two ENSO periodsevents
349 are identical, and the results in Fig. 3 reflect the mean AIS response – potentially biased toward stronger ENSO
350 events – w. We next examine AIS mass change, SMB variability, and the atmospheric circulation driving these
351 changes during different ENSO-dominated periods we defined in this study (see section 2.2)(Figs. 4 and 5). The
352 results reveal distinct spatial patterns of ice mass change associated with individual El Niño and La Niña events.
353 We remind the reader that the GRACE signal is more reliable in the coastal regions and less reliable in the interior,
354 where inherent systematic errors in GRACE measurements in the form of north-south striping are more
355 pronounced.

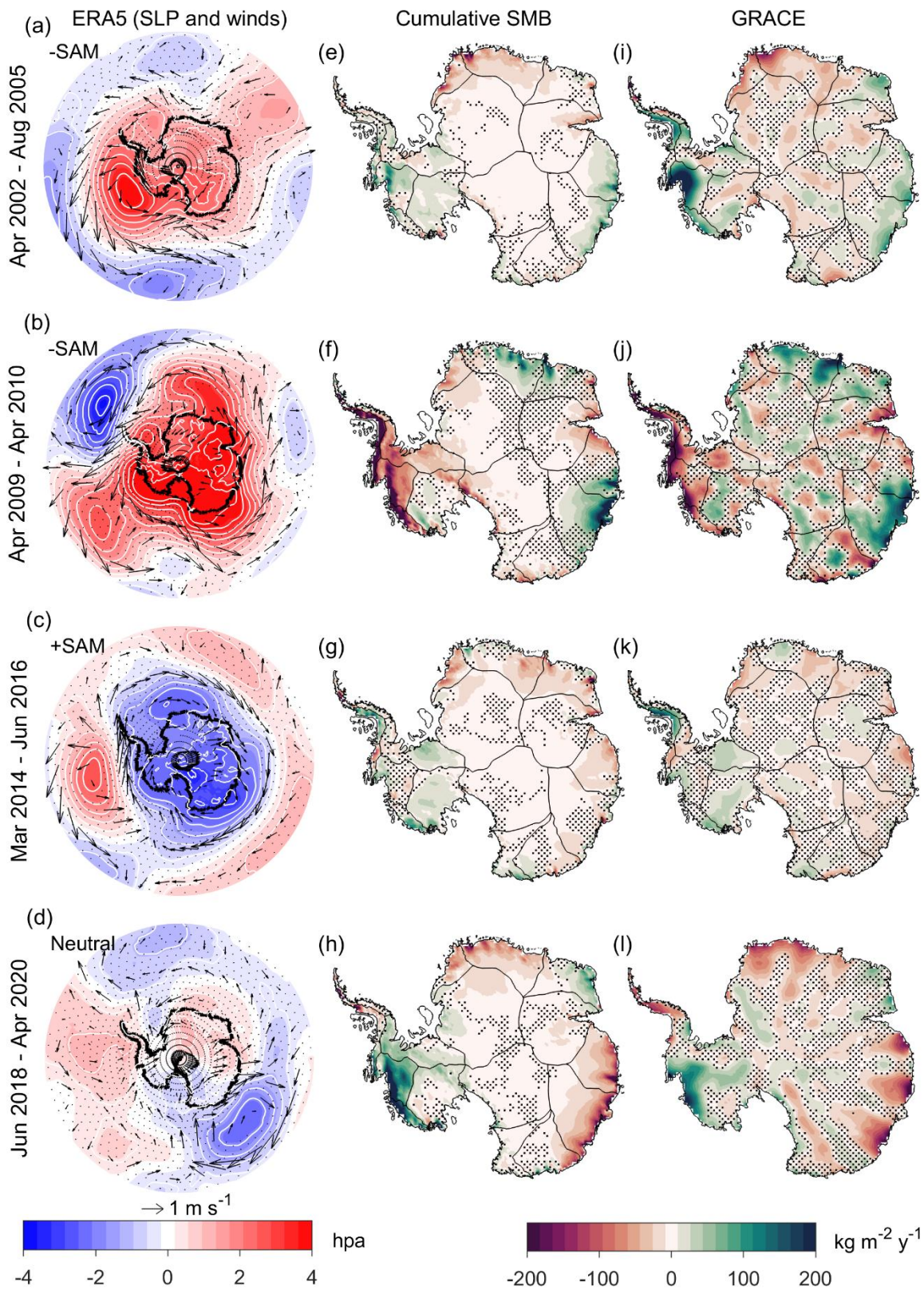
356 **3.2. El Niño-dominated periods**

357 We analyse the variations in atmospheric circulation, SMB, and the resulting ice mass change during each defined
358 El Niño dominated period throughout the GRACE observational record (Fig. 4). Across the Antarctic continent,
359 spatial pressure anomalies vary between El Niño-dominated periods, with both positive and negative pressure
360 anomalies observed (Fig. 4a-d). These pressure patterns reflect-indicate either a relative intensification (high-
361 pressure) or relative weakening (low pressure) of the mean Antarctic ~~h~~High (Fig. 4a-b). These variations align
362 with the cumulatively summed SAM indices (Fig. 1e), where high-pressure anomalies correspond to prolonged
363 negative SAM phases, and low-pressure anomalies coincide with prolonged positive SAM phases. ~~Mass~~
364 ~~anomalies observed in both RACMO SMB and GRACE are most pronounced along the coastal regions, where~~
365 ~~the signals are statistically significant. In this study, we focus on the absolute mass changes during each period,~~
366 ~~while relative impacts are presented in the supplement (Fig. S3).~~

El Niño-dominated periods



El Niño-dominated periods



369 **Figure 4.** Atmospheric circulation anomalies Composite anomaly maps of sea level pressure and 10-m
370 wind from ERA5 reanalysis, representing climatic conditions during El Niño-dominated periods relative
371 to the climatology of the GRACE period (2002–2022) (left), rate of change in cumulative SMB anomalies
372 from RACMO2.4p1 model (middle) and linear rate of GRACE-derived ice mass anomalies (right) during
373 El Niño-dominated period. Sea level pressure anomalies are shown as shaded regions with contours (hPa),
374 while wind anomalies are indicated by reference vectors ($m s^{-1}$). The rate of change in Antarctic SMB is
375 derived from the RACMO2.3p2 model ($kg m^{-2} y^{-1}$), and the rate of surface mass change is obtained from
376 GRACE data ($kg m^{-2} y^{-1}$). SMB and GRACE maps ($kg m^{-2} y^{-1}$) illustrate trends in ice mass variability in
377 AIS mass for each identified El Niño-dominated period. The GRACE signal is more reliable in the coastal
378 regions and less reliable in the interior, where GRACE systematic error in the form of north-south
379 striping is more evident. Non-significant areas are stippled for the pressure anomalies and AIS mass
380 trend at p-value < 0.05.

381 3.2.1. Atmospheric circulation and mass anomalies in West Antarctica anomalies during El Niño- 382 dominated periods

383 In West Antarctica, El Niño-dominated periods are characterised by a high-positive pressure anomaly in the
384 Pacific sector off the West Antarctic coastline, representing a weakened and/or shifted ASL rather than an actual
385 high pressure system (Fig. 4a–b). The position and strength of these is high-positive pressure anomalies varies
386 significantly within for each El Niño-dominated period, which is also reflected in the variation of wind
387 anomalies and spatial patterns of influencing meridional circulation, thus driving distinct spatial patterns in SMB
388 (Fig. 4e–h) and ice mass change (Fig. 4i–l). However, during the 2018–2020 period, no significant pressure
389 anomaly is observed, and in the 2009–2010 period, a significant pressure anomaly is located closer to the continent,
390 with a non-significant pressure anomaly further north (Fig. 4a–b).

391 Considering West Antarctica as two regions, the Amundsen Sea sector and the Antarctic Peninsula, SMB and
392 mass change anomalies during the 2002–2005, 2009–2010, and 2014–2016 El Niño-dominated periods were of
393 different signs but broadly uniform across both sectors (Fig. 4e–g, i–k). Conversely, the 2018–2020 period lacked
394 this uniformity, displaying strong negative anomalies in the Peninsula and strong positive anomalies in the
395 Amundsen Sea sector (Fig. 4h, l). During the earlier three El Niño-dominated periods, the high-pressure anomaly
396 over the Pacific sector extended from the Amundsen to the Bellingshausen Sea (Fig. 4a–c). For the 2018–2020 El
397 Niño-dominated period, the high-pressure anomaly in the Pacific was weaker (closer to climatology) and mainly
398 located in the Bellingshausen Sea (Fig. 4d). These spatial variations demonstrate how the high-pressure anomaly's
399 position significantly influences regional SMB and mass change patterns by controlling meridional circulation.

400 The Amundsen Sea sector exhibits consistent positive SMB (Fig. 4e, g–h) and ice mass anomalies (Fig. 4i, k–l)
401 During three out of four El Niño-dominated periods (2002–2005, 2014–2016, and 2018–2020), the Amundsen
402 Sea sector shows positive anomalies in both SMB (Fig. 4e, g–h) and ice mass anomalies (Fig. 4i, k–l), indicating
403 mass gain, despite variations in the location and strength of the high-positive pressure anomaly in the Pacific (Fig.
404 4a, c–d). Positive SMB and ice mass anomalies predominantly affect the Amundsen Embayment during these
405 periods, with the most pronounced anomalies observed in GRACE data during 2002–2005 (Fig. 4i) and in both
406 SMB and GRACE data during 2018–2020 (Fig. 4h, l). The positive mass anomalies are more widespread across

407 the Amundsen Sea sector during the 2002–2005 period in GRACE (Fig. 4i) and in both SMB and GRACE during
408 the 2018–2020 period (Fig. 4h, l). The positive pressure anomaly in the Pacific which supports these mass gains,
409 is significant during the 2002–2005 period.

410 For the 2014–2016 El Niño-dominated period, we observed weak and, in some regions, non-significant positive
411 SMB and ice mass anomalies in the Amundsen Sea sector and western Ross Sea (Fig. 4g, k) which encompasses
412 the extreme 2015–2016 El Niño event (Bodart and Bingham, 2019) within the GRACE observation period,
413 coincided with weaker positive anomalies in the Amundsen Sea sector compared to the other periods (Fig. 4g, k).
414 During this period, our cumulative ENSO and SAM were uniquely occurred out of phase with (El Niño/+SAM)
415 (Fig. 1e), as evidenced by low-significant negative pressure anomalies over the continent (Fig. 4c) that weakened
416 the Antarctic high. During this period, the high pressure anomaly in the Pacific shifted northward (Fig. 4c), with
417 northerly wind anomalies flow over the Ross and Amundsen Seas corresponding to observed positive anomalies.
418 A low pressure anomaly position between the Ross and Amundsen Seas, contributed to onshore winds and
419 positive anomalies (Fig. 4e). The positive pressure anomaly in the Pacific was located away from the coastline
420 and was associated more with wind anomalies along the shore, rather than onshore (Fig. 4c).

421 The mass change pattern in the Amundsen Sea sector during the 2009–2010 El Niño-dominated period represents
422 a notable exception to the other three periods in regard to is distinct from the other El Niño periods, with
423 widespread significant negative SMB (Fig. 4f) and ice mass (Fig. 4j) change anomalies indicating a net mass
424 reduction. the Amundsen Embayment. Unlike other periods, negative anomalies appeared in the Amundsen
425 Embayment in both SMB and GRACE data (Fig. 4f, j). The characteristic northerly wind flow typically associated
426 with the other El Niño dominated periods in the Amundsen sector was absent. Instead, a high pressure anomaly
427 positioned further west than in the other three periods (between the Amundsen and Ross Seas) generated
428 anomalous southerly winds, resulting in offshore flow from the continent's interior (Fig. 4b). In contrast to the
429 other El Niño periods, a large area of significant positive pressure anomaly extends offshore from the Antarctic
430 continent, spanning from the Peninsula to beyond the Ross Sea, and supports offshore wind anomalies in the
431 Amundsen Sea sector (Fig. 4b).

432 The Antarctic Peninsula exhibits two distinct contrasting mass change variability responses during El Niño-
433 dominated periods (Fig. 4). The 2002–2005 and 2014–2016 El Niño dominated periods show similar responses,
434 with the Peninsula experiencing positive SMB (Fig. 4e, c) and GRACE (Fig. 4i, k) anomalies supported by a high-
435 pressure anomaly in the Pacific driving northerly winds across the region (Fig. 4a, e). Note that the 2002–2005
436 SMB anomaly is only marginally positive (Fig. 4a). In contrast, during the 2009–2010 and 2018–2020 El Niño-
437 dominated periods, southerly wind anomalies prevailed (Fig. 4b, d), resulting in a negative SMB (Fig. 4f) and ice
438 mass anomaly (Fig. 4j) over much of the Peninsula. Also, during the 2009–2010 period, a strong low pressure
439 anomaly over the Weddell Sea induced northerly winds along the eastern Peninsula (Fig. 4b), creating localized
440 positive SMB and ice mass anomalies (Fig. 4f, j). Positive SMB (Fig. 4e, g) and ice mass anomalies (Fig. 4j, l)
441 are observed during the 2002–2005 and 2014–2016 El Niño periods, particularly in GRACE (Fig. 4i, k), whereas
442 negative SMB (Fig. 4f, h) and ice mass anomalies (Fig. 4j, l) are evident during the 2009–2010 and 2018–2020
443 periods. These mass change pattern align with pressure anomaly distributions and are associated with onshore

444 wind anomalies during the 2002-2005 and 2014-2016 periods (Fig. 4a, c) and offshore wind anomalies for 2009-
445 2010 and 2018-2020 (non-significant) periods (Fig. 4b, d).

446 **3.2.2. Atmospheric circulation and mass anomalies in East Antarctic**~~a~~ anomalies during El Niño dominated
447 periods

448 ~~El Niño events have been linked to negative mass anomalies in the East Antarctic Ice Sheet (King et al., 2023; Li~~
449 ~~et al., 2022a), consistent with our earlier findings (Fig. 3b–c). The 2014–2016 and 2018–2020 El Niño dominated~~
450 ~~periods align with this general pattern, showing mostly negative anomalies in SMB (Fig. 4g–h) and GRACE data~~
451 ~~(Fig. 4k–l) across East Antarctica. However, our analysis reveals that the relationship between El Niño and the~~
452 ~~East Antarctic Ice Sheet is not limited to negative mass anomalies, with varying responses observed across the~~
453 ~~Atlantic and Indian Ocean sectors.~~

454 In the Atlantic Ocean sector, Dronning Maud Land, three out of four El Niño-dominated periods (2002-2005,
455 2014-2016, and 2018-2020) consistently showed with negative SMB (Fig. 4e, g–h) and ice mass anomalies (Fig.
456 4i, k–l) anomalies in Dronning Maud Land. The reduction in mass is more extensive during the 2002–2005 and
457 2018–2020 El Niño periods, covering much of Coats Land and Dronning Maud Land, with strong mass anomalies
458 along the western edge of Dronning Maud Land (Fig. 4e, h, i, l). The magnitude of mass reduction is lesser for
459 the 2014-2016 El Niño period (Fig. 4g). The negative anomaly signal during the 2014–2016 El Niño dominated
460 period is weaker compared to the 2002–2005 and 2018–2020 periods, with a weak positive anomaly observed in
461 western Dronning Maud Land. In contrast, the negative anomalies during the 2002–2005 and 2018–2020 periods
462 were more widespread across Dronning Maud Land, with slightly stronger signals in the western areas. However,
463 among these periods, the 2014-2016 El Niño period shows a significant pressure anomaly, which can be directly
464 associated with the observed mass reduction patterns.

465 ~~During the 2002–2005 El Niño dominated period, a low pressure anomaly over the Atlantic extending into~~
466 ~~Dronning Maud Land, combined with a high pressure anomaly over the continent, produced southerly and~~
467 ~~southeasterly winds in Dronning Maud Land (Fig. 4a). Similarly, during 2018–2020, slightly weaker high-~~
468 ~~pressure anomalies over Antarctica induced southerly wind flow off Dronning Maud Land (Fig. 4d). In contrast,~~
469 ~~during 2014–2016, a low pressure anomaly off the Dronning Maud Land coast generated northerly winds into~~
470 ~~western regions supporting slight positive anomalies while southerly winds influenced eastern regions,~~
471 ~~creating differential impacts (Fig. 4e, g, k).~~

472 ~~The 2009–2010 El Niño dominated period exhibits a markedly different response in Dronning Maud Land~~
473 ~~compared to the generally negative mass anomalies observed during other periods. Instead of negative anomalies,~~
474 ~~2009–2010 is characterised by positive mass anomalies (Fig. 4f, j), particularly in eastern Dronning Maud Land,~~
475 ~~as shown in GRACE data (Fig. 4j). A mid-latitude blocking pattern, with a high pressure anomaly extending as a~~
476 ~~ridge to the Antarctic coastline, drives northerly winds onshore (Fig. 4b). Conversely, during the 2009–2010 El~~
477 ~~Niño period, we observed a significant anomalous mass gain in Dronning Maud Land (Fig. 4f, j). This mass gain~~
478 ~~coincides with a significant positive pressure anomaly over the Atlantic, which supports onshore wind anomalies~~
479 ~~into Dronning Maud Land.~~

480 Enderby Land shows positive mass anomalies, which in some instances are evident in GRACE but not in SMB,
481 and vice versa. For example, during the 2002–2005 El Niño period, positive mass anomalies are more pronounced
482 in GRACE than in SMB (Fig. 4e, i), whereas during the 2018–2020 El Niño period, the positive anomalies are
483 stronger in SMB than in GRACE (Fig. 4h, l). Atmospheric circulation anomalies during the 2009–2010 and 2014–
484 2016 El Niño periods are statistically significant and supports the observed mass change patterns. For the 2002–
485 2005 and 2018 El Niño periods, we cannot associate the observed mass patterns to circulation anomalies at the
486 0.05 significance level.

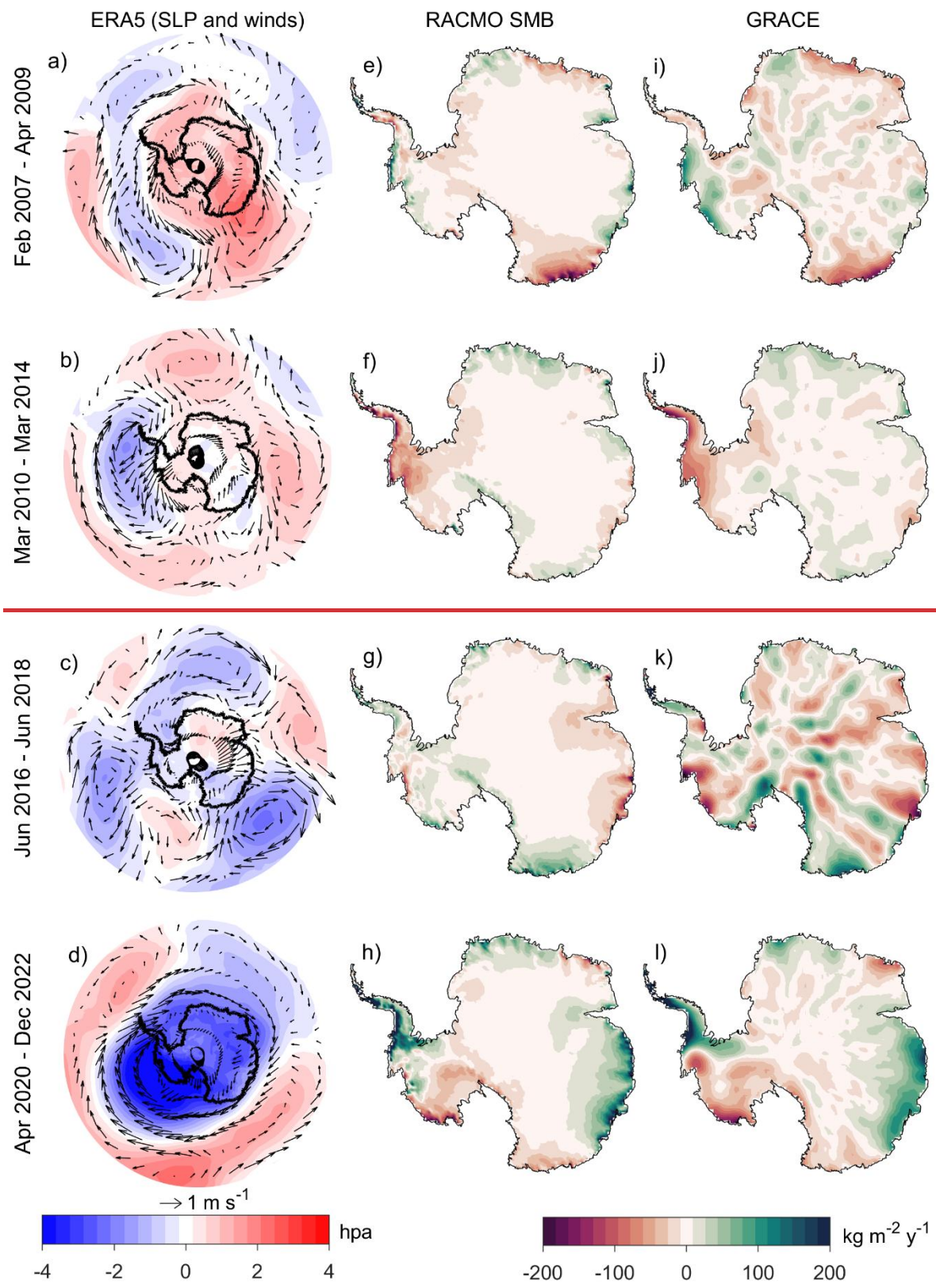
487 In the Indian Ocean sector/Wilkes Land, mass gain is broadly observed during the two distinct response patterns
488 emerge across the four El Niño dominated periods: 2002–2005 and 2009–2010 El Niño periods (Fig. 4e, f, i, j),
489 and a reduction in mass during the coincided with positive SMB (Fig. 4e) and ice mass anomalies (Fig. 4i), while
490 2014–2016 and 2018–2020 El Niño periods (Fig. 4g, h, k, l) correspond to negative anomalies (Fig. 4g–h, k–l).
491 High pressure anomaly over Antarctica during 2002–2005 and 2009–2010 (Fig. 4a, c) align with the negative
492 SAM phase (Fig. 1e), characterised by weakened mid-latitude westerlies and expanded high pressure over
493 Antarctica (Marshall, 2003), which extends northward over Wilkes Land, with circulation patterns inducing
494 northeasterly wind anomalies along the coast (Fig. 4a, c). During the periods with mass gain, positive pressure
495 anomalies were present over Wilkes Land (Fig. 4a, b), with the anomaly more intense and statistically significant
496 during the 2009–2010 El Niño period and associated with a greater magnitude of mass gain in Wilkes Land (Fig.
497 4b, f, j). Conversely, during periods broadly associated with mass reduction (Fig. 4g, h, k, l), negative pressure
498 anomalies were observed around the Wilkes Land region, aligned with offshore wind anomalies across much of
499 the sector (Fig. 4c, d).

500 The 2014–2016 El Niño dominated period aligns with low pressure anomaly over Antarctica and intensified mid-
501 latitude westerlies (Fig. 4e). The low pressure anomaly located over Wilkes Land produces southerly to
502 southwesterly wind anomalies (Fig. 4c), negatively impacting mass balance (Fig. 4g, k). During 2018–2020, weak
503 pressure anomalies over the continent near Wilkes Land accompanied a developing low pressure system in the
504 adjacent ocean (Fig. 4d), intensifying offshore southerly winds and further negatively influencing mass balance
505 (Fig. 4h, l).

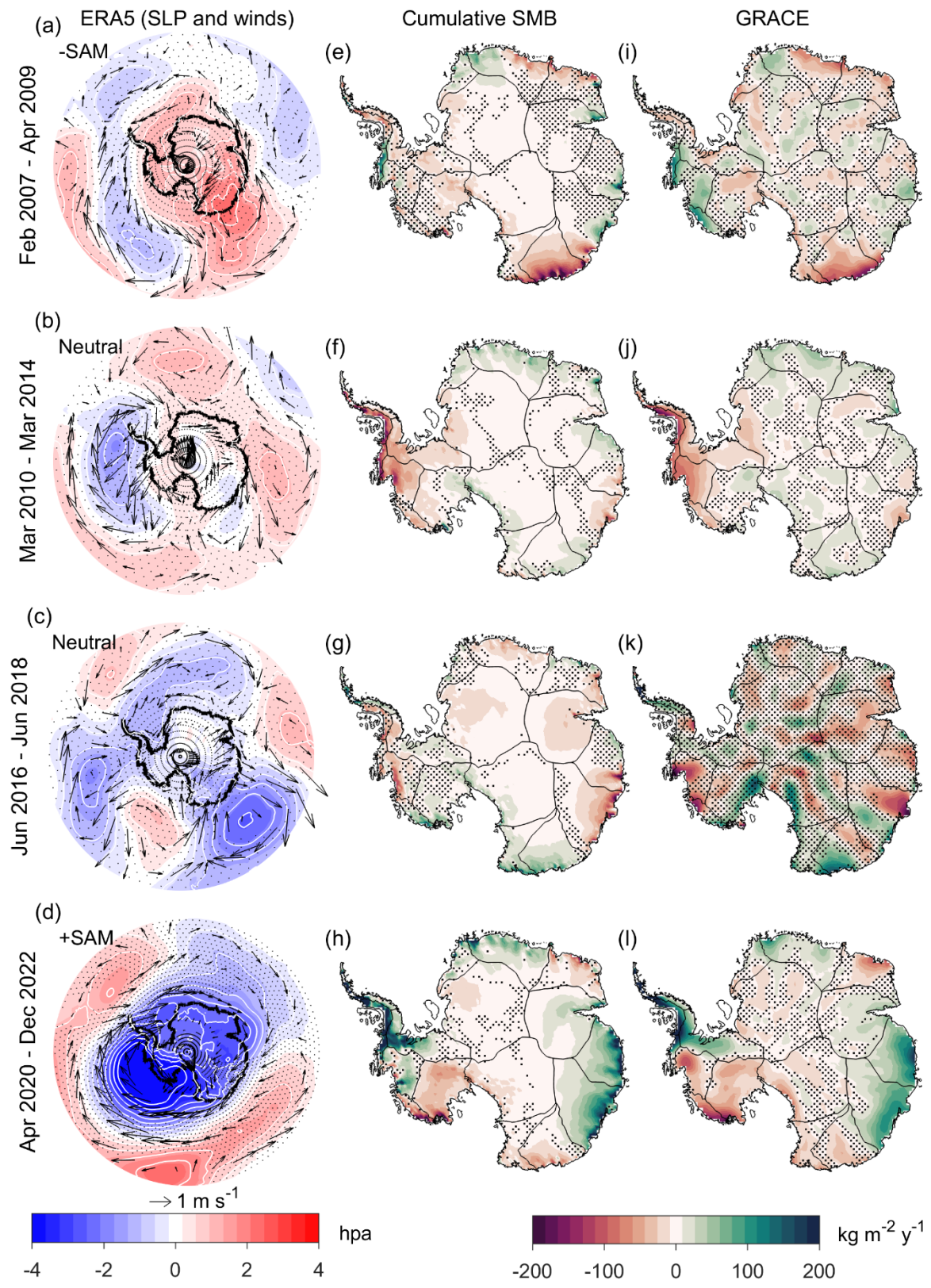
506 **3.3. La Niña-dominated periods**

507 Figure 5 presents atmospheric circulation patterns, SMB anomalies, and AIS mass changes during La Niña-
508 dominated periods. Absolute mass changes are shown in this section, while relative mass changes can be found
509 in the supplementary material (Fig. S3). The atmospheric circulation pattern anomalies during La Niña-dominated
510 periods (Fig. 5a–d) shows fewer areas of statistical significance compared to the El Niño periods (Fig. 4a–d).
511 Instrument malfunctions and the termination of the GRACE mission in 2017 introduced noise and data gaps,
512 affecting ice mass estimates. Therefore, we limit our discussion to the atmospheric circulation and SMB for the
513 2016–2018 La Niña-dominated period to avoid conclusions based on potentially unreliable data in GRACE.

La Niña-dominated periods



La Niña-dominated periods



516 **Figure 5.** Atmospheric circulation anomalies Composite anomaly maps of sea level pressure and 10-m
517 wind from ERA5 reanalysis, representing mean anomaly conditions during La Niña-dominated periods
518 relative to the climatology of the GRACE period (2002–2022) (left), rate of change in cumulative SMB
519 anomalies from the RACMO2.4p1 model (middle), and linear rate of GRACE-derived ice mass anomalies
520 (right) during La Niña-dominated period. Sea level pressure anomalies are shown as shaded regions with
521 contours (hPa), while 10 m wind anomalies are indicated by reference vectors (m s⁻¹). The rate of change
522 in Antarctic SMB is derived from the RACMO2.3p2 model (kg m⁻² y⁻¹), and the rate of surface mass
523 change is obtained from GRACE data (kg m⁻² y⁻¹). SMB and GRACE (kg m⁻² y⁻¹) maps illustrate trends
524 in ice mass variability in ASI mass for each identified La Niña-dominated period. The GRACE
525 signal is strongest near the coastal regions and weaker in the interior, where uncertainties are higher. The
526 GRACE satellite malfunction during 2016–2018 is apparent in the signal for that period, where
527 instrument noise dominates over actual variability with pronounced north-south striping. Non-significant
528 areas are stippled for the pressure anomalies and AIS mass trend at p-value < 0.05.

529 3.3.1. Atmospheric circulation and mass anomalies in West Antarctica anomalies during La Niña- 530 dominated periods

531 Overall, during our La Niña-dominated periods, the Pacific sector exhibits a persistent negative pressure anomaly
532 (Fig. 5a–d), which appears more elongated than the positive pressure anomaly associated with El Niño periods.
533 This pressure anomaly is statistically significant for the 2020–2022 La Niña period; however, there are also
534 significant regions near the centre of the pressure anomaly during the 2010–2014 La Niña period. are
535 characterised by a low pressure anomaly in the Pacific sector, reflecting a strengthening and/or shift of the ASL
536 (Fig. 5a–d). Our analysis reveals variable mass changes in West Antarctica between the Amundsen sector and
537 Antarctic Peninsula, with a notable exception during 2010–2014, when a uniformly negative response was
538 observed (Fig. 5f, j). During this period, the low pressure anomaly in the Pacific sector extended from the
539 Bellingshausen to Amundsen Seas (Fig. 5b). In contrast, other La Niña dominated periods exhibited a bipolar
540 mass pattern between the Amundsen sector and Antarctic Peninsula (Fig. 5e, g–h), with a less elongated low-
541 pressure anomaly in the Pacific (Fig. 5a, c–d).

542 The low pressure anomaly in the Pacific during these La Niña dominated periods enhanced southerly wind
543 anomalies off the Amundsen Embayment, with broadly negative SMB (Fig. 5f, g–h) and ice mass anomalies (Fig.
544 5j, k–l) consistent across the 2010–2014, 2016–2018, and 2020–2022 La Niña dominated periods. The 2007–
545 2009 La Niña dominated period, however, showed a broadly positive ice mass anomaly in the Amundsen
546 Embayment (Fig. 5e, i) more typical of most El Niño dominated periods as described previously due to a
547 northwest shift of the low pressure anomaly in the Pacific (compared to the other three La Niña dominated
548 periods) (Fig. 5a). Around the Bellingshausen and Amundsen Seas, there is an interaction between northerly winds
549 from the Pacific and southerly winds from the continent that potentially can support convection and positive mass
550 anomalies (Fig. 5a). Three out of the four La Niña periods (2010–2014, 2016–2018, and 2020–2022) are broadly
551 associated with negative SMB (Fig. 5f–h) and ice mass anomalies (Fig. 5j–l) across the Amundsen Sea sector.
552 The reduction in mass during the 2020–2022 and 2010–2014 La Niña periods aligns with a significant negative
553 pressure anomaly in the Pacific sector, and offshore wind anomalies (Fig. 5b, d).

555 In contrast, during the 2007–2009 La Niña period, a mass gain is prominently observed in GRACE (Fig. 5i), a
556 pattern more commonly associated with El Niño periods described earlier. However, the SMB and pressure
557 anomaly patterns during this period are not statistically significant at the 0.05 level.

558

559 The spatial impact of the Antarctic Peninsula mass responses during La Niña dominated periods also exhibits
560 variation, with both positive and negative mass anomalies observed across different La Niña dominated periods.
561 The 2007–2009 and 2010–2014 La Niña dominated periods showed negative mass anomalies (Fig. 5e–f, i–j),
562 while 2016–2018 and 2020–2022 La Niña dominated periods exhibited positive anomalies (Fig. 5g–h, k–l). The
563 widespread mass reduction during the 2010–2014 La Niña dominated period, evident in both SMB and GRACE
564 data (Fig. 5f, j), coincided with the strongest La Niña event in the GRACE record. Southerly winds prevailed
565 across the Peninsula during mass loss periods (2007–2009, 2010–2014) (Fig. 5a–b), whereas northerly winds
566 dominated during mass gain periods (2016–2018, 2020–2022) (Fig. 5g–h). Similar to the Amundsen Sea sector,
567 the Antarctic Peninsula exhibits contrasting mass change responses during La Niña-dominated periods. Broadly,
568 negative mass anomalies are observed during the 2007–2009 and 2010–2014 La Niña periods (Fig. 5i, j), whereas
569 positive mass anomalies are evident during the 2016–2018 and 2020–2022 La Niña periods (Fig. 5k, l). The
570 magnitude of mass reduction is strongest during the 2010–2014 La Niña period, while the mass gain is most
571 pronounced during the 2020–2022 La Niña period.

572 The 2020–2022 La Niña dominated period stands out as the only one coinciding with a positive SAM phase (Fig.
573 1d, e), featuring an anomalous deepening of the low pressure anomaly in the Pacific ASL. This intensified low-
574 pressure anomaly drove strong northerly wind anomalies over the Antarctic Peninsula (Fig. 5d). This contrasting
575 mass change response between the two periods aligns with the position of the negative pressure anomaly in the
576 Pacific sector. In the 2010–2014 La Niña period, the pressure anomaly is centred over the Bellingshausen Sea,
577 accompanied by offshore wind anomalies over the Peninsula (Fig. 5b). In contrast, during the 2020–2022 La Niña
578 period, the negative pressure anomaly is centred in the Amundsen Sea, with onshore wind anomalies directed into
579 the Peninsula (Fig. 5d).

580 3.3.2. Atmospheric circulation and mass anomalies in East Antarctic ~~a~~ anomalies during La Niña- 581 dominated periods

582 The East Antarctic coastline experienced widespread positive SMB anomalies during the 2010–2014 and 2020–
583 2022 La Niña dominated periods (Fig. 5f, h), while the 2007–2009 and 2016–2018 La Niña dominated periods
584 showed regionally variable responses across the Atlantic and Indian Ocean sectors (Fig. 5e, g). In Dronning Maud
585 Land, SMB (Fig. 5f, h) and GRACE derived (Fig. 5j, l) mass anomalies were consistently positive during 2010–
586 2014 and 2020–2022 La Niña dominated periods, whereas 2007–2009 La Niña dominated period showed
587 contrasting responses—positive mass anomalies in the west and negative mass anomalies in the east (Fig. 5e).
588 Along the Atlantic sector, a dipole-like mass anomaly pattern is present during the 2007–2009 and 2020–2022 La
589 Niña periods (Fig. 5e, h), whereas a more uniform response is observed during the 2010–2014 and 2016–2018 La
590 Niña periods (Fig. 5f, g). During the 2007–2009 La Niña period, positive SMB anomalies were observed over
591 Coats Land and negative SMB anomalies toward Enderby Land (Fig. 5e), with this spatial pattern reversed during
592 the 2020–2022 La Niña period (Fig. 5h).

593
594 Positive mass anomalies were also observed across the Atlantic region during the 2014–2016 La Niña period,
595 with a reversed pattern during the 2016–2018 La Niña period. Regionally, Dronning Maud Land shows consistent
596 positive SMB (Fig. 5f, h) and ice mass anomalies (Fig. 5j, l) during the 2010–2014 and 2020–2022 La Niña
597 periods.

598 These varying impacts in Dronning Maud Land stem from the positioning of positive pressure anomaly in the
599 Atlantic Ocean. During 2007–2009, a high pressure anomaly west of Dronning Maud Land flow, generating
600 northerly winds in the west and southerly winds offshore in the east (Fig. 5a), creating spatial heterogeneity in
601 mass change (Fig. 5e). In 2010–2014, the high pressure anomaly was farther north (Fig. 5b), resulting in uniform
602 northerly winds and positive mass anomalies across the region (Fig. 5f). The 2020–2022 period, marked by an
603 anomalously deep low pressure anomaly in the Pacific, also featured strong northerly winds over Dronning Maud
604 Land (Fig. 5d). The negative pressure anomaly during the 2020–2022 La Niña period aligns with the observed
605 mass gain in Dronning Maud Land. Conversely, during the 2016–2018 period, negative SMB anomalies were
606 observed in Dronning Maud Land, with no clear pressure anomaly pattern (Fig. 5g).

607 In the Indian Ocean sector/Wilkes Land we found no consistent mass response to exhibited two distinct SMB
608 responses across La Niña-dominated periods. During the 2020–2022 La Niña period, mass change in the Indian
609 Ocean sector is spatially uniform, with positive mass anomalies observed across the entire region (Fig. 4h, l). This
610 contrasts with other La Niña periods, which show more variable responses.

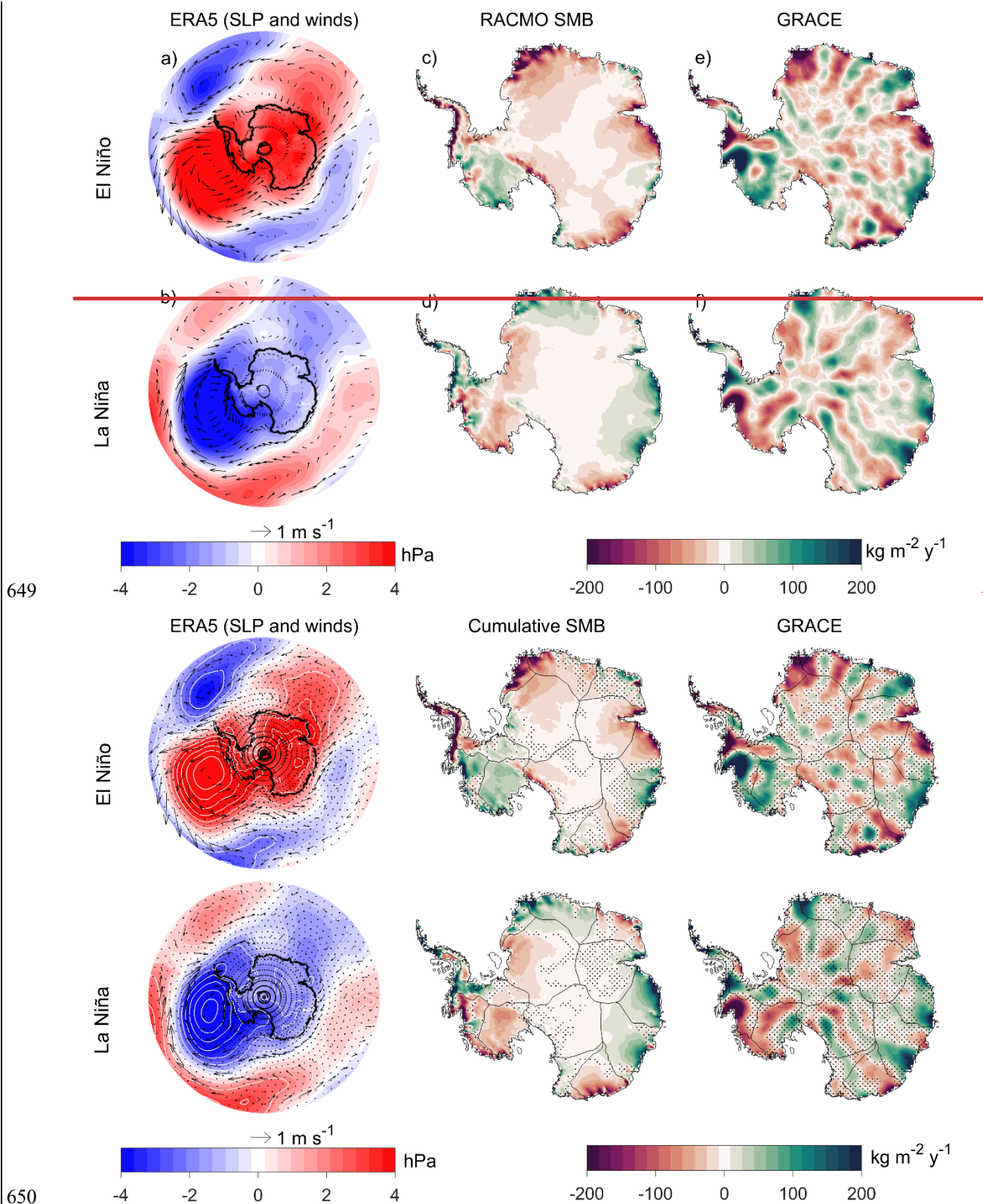
611 Positive SMB anomalies occurred in 2007–2009 and 2020–2022 (Fig. 5e, h), while 2010–2014 and 2016–2018
612 were associated with negative SMB anomalies (Fig. 5j, l)). The 2007–2009 period featured ridging of the Antarctic
613 high, inducing northerly wind anomalies that support moisture transport into the region (Fig. 5a). In contrast,
614 during 2010–2014, a weaker low pressure anomaly generated southerly wind anomalies (Fig. 5b), likely
615 suppressing moisture transport and leading to negative mass anomalies (Fig. 5f, l). The 2010–2014 and 2016–
616 2018 La Niña periods are consistent with each other, showing negative mass anomalies over Wilkes Land. For
617 both periods, a negative pressure anomaly is present adjacent to the Wilkes Land coast, with the 2016–2018 period
618 showing a statistically significant anomaly and stronger negative mass signals. In contrast, the 2007–2009 and
619 2020–2022 La Niña periods are associated with positive mass anomalies in Wilkes Land (Fig. 5i, l), although the
620 anomalies during 2007–2009 are weaker and less spatially extensive (Fig. 5i). During the 2007–2009 La Niña
621 period, a positive pressure anomaly marginally significant at the centre of the anomaly extends offshore along the
622 Wilkes Land coast, associated with onshore wind anomalies (Fig. 5a).

623 The 2020–2022 La Niña dominated period is distinct due to the anomalous deepening of the low pressure
624 anomaly in the Pacific, which induced strong northerly to northwesterly winds over Wilkes Land (Fig. 5d),
625 contributing to a pronounced positive mass anomaly (Fig. 5h, l). However, this period also includes extreme events
626 such as the March 2022 atmospheric river event, which delivered record breaking precipitation (Wille et al., 2024;
627 Wille et al., 2022; Wille et al., 2021). This raises the question of whether the combination of La Niña and positive
628 SAM increases the likelihood of such extremes, while also considering the potential impact of climate change.
629 However, we note that there is only one example of these conditions co-occurring during the GRACE observation
630 period.

631 **3.4. Mean Anomalies during ENSO-dominated periods**

632 Figure 6 presents the mean AIS response across El Niño- and La Niña-dominated periods, summarizing the
633 impacts of different ENSO ~~event~~ periods. ~~The figure is derived by averaging the maps presented in Figures 4 and~~
634 ~~5.~~ While this mean response differs slightly from the regression results in Fig. 3b–c, certain regional patterns
635 remain consistent. ~~From the GRACE results, it is obvious north-south striping noise in GRACE observations is~~
636 ~~maximised over short periods. The~~ SMB results show a positive response ~~during El Niño-dominated periods~~ in
637 the Amundsen Sea sector ~~and Marie Byrd Land, as well as in Enderby Land (Fig. 6c). In contrast, negative SMB~~
638 ~~anomalies are observed in the Antarctic Peninsula, Coats Land, and Dronning Maud Land (Fig. 6c). During El~~
639 ~~Niño-dominated periods and a negative response during La Niña-dominated periods, with the opposite~~ this pattern
640 ~~is broadly reversed (Fig. 6d). Wilkes Land shows positive SMB anomalies during both El Niño- and La Niña-~~
641 ~~dominated periods; however, the anomalies are more spatially extensive during La Niña (Fig. 6c, d) in the Antarctic~~
642 ~~Peninsula and Dronning Maud Land. The patterns in GRACE are broadly similar to the SMB results, however,~~
643 ~~north-south striping noise in GRACE is maximised over short periods.~~

644 ~~However, averaging multiple ENSO-dominated periods may obscure variability and lead to misinterpretation. As~~
645 ~~shown in Figs. 4e–h and 5e–h, mass variability – particularly in the Antarctic Peninsula and East Antarctica –~~
646 ~~varies significantly across individual ENSO events. The mean response fails to capture these short-term variations,~~
647 ~~which are critical for understanding their influence on AIS mass balance.~~



651 **Figure 6.** The composites are generated based on the results of the four defined ENSO-dominated periods
652 combined integrated spatial anomalies of climatic variables, RACMO SMB, and GRACE-derived ice
653 mass change for the four El Niño and La Niña dominated periods. ERA5 mean seal level pressure and 10
654 m wind anomalies (left), RACMO2.4p1 SMB (centre), and GRACE-derived ice mass change (right). This
655 represents the cumulative impact of different ENSO phases on AIS mass variability. Sea level pressure

656 anomalies are shown as shaded regions with contours (hPa), and 10 m wind anomalies are indicated
657 vectors (m s^{-1}). SMB and GRACE ($\text{kg m}^{-2} \text{y}^{-1}$) are shown. Non-significant areas stippled at p-value<0.05.

658 **4. Discussion**

659 **4.1 Continental-wide perspective**

660 We examined the AIS mass variability during different ENSO-dominated periods. Our results show that the AIS
661 exhibits considerable variability across these periods, each associated with its own circulation anomalies (Figs. 4,
662 5), influenced by interactions between ENSO and SAM (Hosking et al., 2013; Fogt et al., 2011). Over longer
663 timescales, the mean response reveals a dipole pattern: positive mass anomalies in West Antarctica and negative
664 anomalies in East Antarctic during El Niño periods, with the reverse during La Niña periods (Fig. 3b, c). This
665 pattern is supported by data-driven analysis showing a strong correlation between GRACE and cumulative ENSO
666 indices (King et al., 2023). in response to ENSO forcing is complex, as it impacts southern high latitude
667 atmospheric circulation, which in turn influences precipitation and Antarctic SMB (King et al., 2023; Li et al.,
668 2022a). Our results are consistent with previous studies, indicating that changes in atmospheric circulation linked
669 to both ENSO and SAM drives the short term AIS mass variability (Clem et al., 2016; Zhan et al., 2021; Zhang
670 et al., 2021). The El Niño and La Niña dominated periods we examined exhibited consistent spatial patterns of
671 ice mass change during most periods across Antarctica, with mass gain in West Antarctica and mass decrease in
672 East Antarctica during El Niño dominated periods and the reverse pattern during La Niña dominated periods.
673 This pattern has been identified in previous studies using GRACE (King et al., 2023; Zhang et al., 2021).

674 However, there is a difference between the SMB signal and GRACE in West Antarctica, but they are closely
675 aligned in East Antarctica (Fig. 3b, c). This suggests that SMB variability drives of ice mass changes in East
676 Antarctica, but not necessarily in West Antarctica. The difference may be due to the near-instantaneous response
677 of ice dynamics to ENSO-driven oceanic forcing and/or mismodelled SMB (IMBIE Team, 2018; Rignot et al.,
678 2019), with the latter being more likely (King and Christoffersen, 2024).

679 However, our results reveal varied spatial patterns during different ENSO dominated periods, not all consistent
680 with the previously reported bipolar ENSO spatial pattern (Li et al., 2022a; King et al., 2023). This bipolar spatial
681 pattern likely represents the underlying ENSO impact on the AIS, supported by the published purely data driven
682 analyses of GRACE data, showing strong correlation with cumulative ENSO indices (King et al., 2023). Our
683 analysis suggests significant deviations from this pattern during some ENSO dominated periods. Averaging
684 multiple ENSO-dominated periods can obscure variability associated with individual periods and lead to
685 misinterpretation. As shown in Figs. 4e–h and 5e–h, mass variability—particularly in the Antarctic Peninsula and
686 East Antarctica—varies significantly across individual ENSO events (Figs. 4, 5). The mean response fails to
687 capture these short-term variations, which are critical for understanding their influence on AIS mass balance.

688 The interaction between ENSO strength, duration, SAM phase, and the ASL response is crucial in determining
689 AIS mass variability. These factors influence atmospheric circulation patterns and subsequently affect ice mass
690 variability across different Antarctic regions. It is noteworthy that the period from 2000 to 2020 has been

691 characterised by unusual Antarctic climate dynamics, attributed to changes in large scale circulation patterns that
692 have significantly altered climate patterns across the continent (Xin et al., 2023).

693 4.2 West Antarctica

694 4.2.1 El Niño-dominated periods

695 El Niño-and La Niña-dominated periods correspond to positive and negative pressure anomalies in the Pacific,
696 respectively, indicative of positive PSA-1 and negative PSA-1 patterns (Hoskins and Karoly, 1981). These
697 patterns are associated with a weakened or strengthened ASL, influencing circulation and climate in West
698 Antarctica (Raphael et al., 2016a; Turner et al., 2017; Turner et al., 2012). The spatial SMB and mass change
699 patterns we observed across the West Antarctic Ice Sheet largely correspond to the position and intensity of the
700 ASL (Raphael et al., 2016a). The Positive ice mass anomalies in the Amundsen Sea sector during the 2002-2005,
701 2014-2016 and 2018-2020 El Niño-dominated periods (Fig. 4i, k-l) and negative anomalies during the 2010-2014
702 and 2020-2022 La Niña periods (excluding the 2016-2018 period due to noisy GRACE data) showed mass gain
703 patterns, especially in the Amundsen Sea region (Fig. 4e, g-h) (Fig. 5i, k-l), are broadly consistent with previous
704 studies (Paolo et al., 2018; King et al., 2023). This positive mass anomaly pattern is supported by the atmospheric
705 circulation during these periods (Fig. 4a, c-d), as ASL variability modulates moisture transport into the Amundsen
706 Sea sector and the Antarctic Peninsula (Raphael et al., 2016a). These mass anomalies are supported by the
707 variability in the ASL during El Niño and La Niña periods influencing circulation into the Amundsen Sea sector.

708 During El Niño conditions, a the weakening of the ASL and reduced coastal easterlies reduces Ekman transport
709 of cold surface water onto the continental shelf, enhances on shelf transport of warm Circumpolar Deep Water,
710 and leads to subsurface warming of the continental shelf. Westerly wind anomalies to bring marine air masses,
711 onshore, which, enhance snowfall and mass accumulation through orographic lifting (Paolo et al., 2018; Huguenin
712 et al., 2024). Despite increased basal melting during El Niño events, high snow accumulation from moisture laden
713 winds undergoing orographic lifting offsets mass loss at the surface, contributing to a positive mass anomaly
714 (Huguenin et al., 2024). Our results support these findings, as three out of four El Niño dominated periods show
715 a positive anomaly in the Amundsen Sea sector, as seen in both SMB and GRACE. In contrast, La Niña conditions
716 strengthen the ASL and intensify coastal easterlies, limiting moisture transport and reducing precipitation
717 (Huguenin et al., 2024; Hosking et al., 2013).

718
719 However, the 2009–2010 El Niño period deviates from this pattern, with negative SMB anomalies observed in
720 the Amundsen Sea sector (Fig. 4f). The pressure anomaly during this period is distinct, with a positive pressure
721 anomaly extending from the Amundsen Sea to beyond the Ross Sea. An important difference to the other El Niño
722 periods, is the extension of this positive pressure anomaly further to the west, which decreases moisture transport
723 into the region. This period encompasses a strong Central Pacific El Niño event (Kim et al., 2011), and associated
724 pressure anomaly (Fig. 4b) resembles patterns linked to such events, which are associated with moisture depleted
725 wind anomalies and suppressed precipitation in the Amundsen and Bellingshausen regions (Chen et al., 2023;
726 Macha et al., 2024).

727 The mass gain in these 2002–2005, 2014–2016 and 2018–2020 El Niño-dominated period in the Amundsen sector
728 differ from findings reported by Macha et al. (2024), who noted an increase in snow accumulation in the western

729 ~~Ross Sea sector and a decrease in the Amundsen Sea sector for both central and eastern Pacific El Niño events.~~
730 ~~This discrepancy stems from methodological differences: our analysis focuses on the net mass change over entire~~
731 ~~ENSO-dominated periods (defined using the Niño 3.4 index), whereas Macha et al. (2024) utilised the central and~~
732 ~~eastern El Niño indices provided by and concentrated on seasonal mass changes during the peak (JJA and SON)~~
733 ~~of these ENSO events. By considering entire periods rather than just peak phases, our approach captures the net~~
734 ~~mass change throughout complete events, providing important context for overall ice sheet mass balance.~~

735 ~~Our results from the 2009–2010 El Niño-dominated period show a pattern across the atmospheric circulation,~~
736 ~~SMB and GRACE that is more typical of La Niña events (Fig. 4b, f, j), with offshore winds and a decrease in ice~~
737 ~~mass observed in West Antarctica. This is unexpected since El Niño events typically enhance moisture transport~~
738 ~~into West Antarctica (Huguenin et al., 2024). This period has been characterised as a strong Central Pacific El~~
739 ~~Niño (Kim et al., 2011), and the anomalous response can be attributed to altered Rossby wave propagation from~~
740 ~~the tropical Pacific into Antarctica (Chen et al., 2023). This shift generates an anticyclone in the Ross–Amundsen~~
741 ~~seas, inducing southerly flow, which reduces precipitation between the Amundsen and Bellingshausen regions~~
742 ~~(Chen et al., 2023). Our SMB pattern for the 2009–2010 El Niño-dominated period, particularly in West~~
743 ~~Antarctica, aligns closely with the influence of Central Pacific El Niño events on Antarctic SMB as described by~~
744 ~~Macha et al. (2024). Our 2009–2010 El Niño mass pattern aligns with Macha et al. (2024), who reported reduced~~
745 ~~accumulation during Central Pacific El Niño events in the SON and JJA seasons. These similarities suggest that~~
746 ~~the observed mass change may reflect the impact of Central Pacific El Niño phases during the SON and JJA~~
747 ~~seasons in the Amundsen Sea sector.~~

748 ~~It is important to state that our defined ENSO periods do not distinguish between El Niño types or seasonal phases~~
749 ~~but instead capture the net mass change over the entire period, providing broader context for ice sheet mass~~
750 ~~balance.~~

751 ~~Similarly, the 2007–2009 La Niña period shows a mass pattern that contrasts with other La Niña periods, featuring~~
752 ~~a positive mass anomaly in the Amundsen Sea sector (Fig. 5i). However, atmospheric circulation patterns during~~
753 ~~this period do not statistically support the observed mass gain, suggesting that it may be linked to unrelated~~
754 ~~weather events or other modes of climate variability.~~

755
756 ~~The Antarctic Peninsula's response to El Niño-dominated periods shows considerable variability in SMB and ice~~
757 ~~mass changes. This variability is closely linked to large-scale climate modes, such as SAM and ENSO (Clem et~~
758 ~~al., 2016), as well as the Peninsula's unique geography, which is marked with by the presence of a mountain range.~~
759 ~~SAM particularly affects westerly winds and associated moisture delivery to the Peninsula, especially its western~~
760 ~~side (Orr et al., 2008).~~

761 ~~During the 2002–2005 and 2014–2016 El Niño-dominated periods (Fig. 4a, e), westerly winds transported moisture~~
762 ~~onto the western side of the Peninsula, leading to increased precipitation through orographic lifting and resulting~~
763 ~~in positive SMB and ice mass anomalies. The westerlies were particularly strong during the 2014–2016 period~~
764 ~~due to the prevailing positive phase of SAM, which enhanced moisture transport and contributed to a stronger~~
765 ~~positive SMB anomaly compared to the 2002–2005 period.~~

766 On the eastern side of the Peninsula, westerlies typically induce foehn winds (Clem et al., 2016; Clem and Fogt,
767 2013), reducing SMB and ice mass. This pattern was present during both the 2002–2005 and 2014–2016 El Niño-
768 dominated periods, though the signal remained relatively weak (Fig. 4e, g). In contrast, the sustained influx of
769 moisture from the deepened ASL during the 2020–2022 La Niña-dominated period favoured precipitation, leading
770 to positive SMB anomalies and net ice mass gain. Our results support that mass variability in the Antarctic
771 Peninsula is variable and influenced by various factors such as large-scale climate modes including SAM and
772 ENSO (Clem et al., 2016; Clem and Fogt, 2013) and the Peninsula's unique mountainous geography. A previous
773 study demonstrated a reduction in mass during El Niño and an increase during La Niña across the Peninsula
774 (Sasgen et al., 2010). This is consistent with our results for the 2018–2020 El Niño- and 2020–2022 La Niña-
775 dominated periods (Figs. 4l, 5l). Meanwhile, other studies suggest the opposite pattern, reporting an increase in
776 mass during El Niño and a reduction during La Niña in the Peninsula (Zhang et al., 2021), which aligns with our
777 observed ice mass change during the 2002–2005 and 2014–2016 El Niño periods (Fig. 4i, k) and 2010–2014 La
778 Niña period (Fig. 5j). However, the variable impact appears to be influenced by the position and orientation of the
779 ASL and its effect on moisture transport into the Peninsula (Raphael et al., 2016b). Further, moisture transport
780 into the Peninsula is influenced by SAM-driven westerly winds and ENSO-related meridional flow (Orr et al.,
781 2008; Clem et al., 2016), which contributes to the complex mass change patterns.

782 **4.2.2 La Niña dominated periods**

783 La Niña dominated periods showed varied effects (Fig. 5). Two out of three La Niña dominated periods we
784 considered (excluding the noisy GRACE solution during the 2016 2018 La Niña dominated period) display a
785 consistent spatial pattern, with negative mass anomalies in the Amundsen Sea region (Fig. 5j, l), aligning with
786 previous studies (Paolo et al., 2018; King et al., 2023; King and Christoffersen, 2024). The strengthening of the
787 ASL during La Niña conditions enhances coastal easterly anomalies in West Antarctica (Fig. 5b, d), increases
788 Ekman transport of cold surface water onto the ice shelf, and reduces the on shelf transport of warm Circumpolar
789 Deep Water and moisture laden winds, leading to reduced precipitation in West Antarctica (Huguenin et al.,
790 2024). The intensification of the ASL during La Niña events inhibits moisture influx into the region by promoting
791 offshore winds (Hosking et al., 2013), resulting in reduced precipitation, SMB, and ice mass decline in West
792 Antarctica (King et al., 2023; Zhang et al., 2021). However, a positive mass anomaly occurs in the Amundsen Sea
793 sector during the 2007 2009 La Niña dominated period, contrasting with other La Niña dominated periods (Fig.
794 5i). This highlights the fact that ENSO is not the sole driver of ice mass variability in West Antarctica, though our
795 analysis is limited in isolating ENSO signals in the region. The positive mass anomaly may potentially be tied to
796 the interaction between the northerly and southerly winds, which form a convergence zone that enhances
797 precipitation (Fig. 5a).

798 Ice mass variability in the Antarctic Peninsula is complex, as ENSO and SAM influence on circulation patterns
799 differs spatially and seasonally in terms of temperature variability (Clem et al., 2016; Clem and Fogg, 2013).
800 ENSO conditions tend to promote meridional circulation, especially during winter, while SAM favours zonal
801 circulation. Together, these create complex effects on Antarctic Peninsula climate. Studies report decreased SMB
802 along the Bellingshausen Sea Antarctic Peninsula during El Niño, with an increase in the Amundsen Sea sector,
803 while the reverse occurs during La Niña (Sasgen et al., 2010). This spatial pattern is consistent with our results
804 for the 2018 2020 El Niño and 2020 2022 La Niña dominated periods (Figs. 4l and 5l). Other studies have
805 reported a uniform impact spanning from the Amundsen Sea sector to the Antarctic Peninsula (Zhang et al., 2021),
806 which aligns with our observed ice mass change during the 2014 2016 El Niño and 2010 2014 La Niña dominated
807 periods (Figs. 4g and 5j). The impact of ENSO between the Amundsen Sea sector and Antarctic Peninsula depends
808 on the location and extent of the ASL between the Ross and Bellingshausen Seas (Raphael et al., 2016b). During
809 La Niña, the ASL tends to elongate, with its centre often located further west compared to its position during El
810 Niño (Huguenin et al., 2024), and a broader ASL leads to more uniform impact across West Antarctica (Clem and
811 Fogg, 2013), as observed during the 2010 2014 La Niña dominated periods.

812 **4.3 East Antarctica**

813 In East Antarctica, moisture transport appears primarily influenced by the strength and position of cyclonic and
814 anticyclonic anomalies over the continent and the Southern Ocean (Figs. 4a d and 5a d). These pressure
815 anomalies regulate atmospheric circulation, with changes in the meridional atmospheric flow affecting heat and
816 moisture distribution across the region (Scarchilli et al., 2011; Wang et al., 2024; Udy et al., 2021). The pressure
817 anomaly over the Antarctic continent is largely governed by the SAM phase, which modulates the positioning of
818 cyclonic and anticyclonic anomalies over both the continent and Southern Ocean, establishing SAM as a key
819 driver of East Antarctic Ice Sheet variability. El Niño and La Niña events have been linked to negative and positive
820 cumulative mass anomalies, respectively in the East Antarctic Ice Sheet (King et al., 2023; Li et al., 2022a).

821 consistent with our earlier findings (Fig. 3b–c). Our 2014–2016, 2018–2020 El Niño periods (Fig. 4k, l) and 2010–
822 2014, 2020–2022 La Niña periods (Fig. 4j, l) broadly align with this pattern. However, this pattern is consistent
823 for every ENSO period (e.g. Fig. 4j 5i), and in some periods regionally variable responses observed across the
824 Atlantic and Indian Ocean sectors.

825 SMB anomalies in East Antarctica are primarily influenced by the strength and position of cyclonic and
826 anticyclonic anomalies over the continent and the Southern Ocean (Figs. 4a–d and 5a–d). These pressure
827 anomalies regulate atmospheric circulation, with meridional flow changes affecting heat and moisture distribution
828 across the region (Scarchilli et al., 2011; Wang et al., 2024; Udy et al., 2021). The SAM phase largely governs
829 these pressure patterns, modulating their positioning and highlighting its role as dominant climate driver in East
830 Antarctica (Fogt et al., 2012; Fogt and Marshall, 2020b; Marshall et al., 2013). For instance, 2014–2016 El Niño
831 showed a spatial mass pattern that are consistent with a positive SAM phase, with a reduction in precipitation
832 (Marshall et al., 2017) and observed negative mass anomaly (Fig. 4g).

833 The anomalous mass gain during the 2009–2010 El Niño period observed in Dronning Maud Land has been
834 attributed to atmospheric blocking, which produced large episodic snowfall events (Boening et al., 2012).
835 Similarly, a positive pressure anomaly in the Atlantic during the 2010–2014 La Niña period (although not
836 significant at $p < 0.05$ over the 4-year period) appears to support the mass gain in the Dronning Maud Land (Fig.
837 5j). Atmospheric blocking favours the occurrence of atmospheric rivers reaching the Antarctic coastline, often
838 associated with increased precipitation and temperature (Wille et al., 2021; Pohl et al., 2021). The weakening of
839 the westerlies during negative SAM conditions (Clem et al., 2016), allows for Rossby wave amplification and an
840 increased frequency of atmospheric blocking events in East Antarctica, particularly during winter, when the
841 relationship is strongest (Wang et al., 2024). It is important to note that climate modes of variability can create
842 conditions favourable for atmospheric river events in East Antarctic (Shields et al., 2022), especially in Wilkes
843 Land (Wang, 2023). However, in Dronning Maud Land, atmospheric rivers explain about 77 % of interannual
844 variability (Baiman et al., 2023)

845 Our 2002–2005 and 2009–2010 El Niño periods, along with the 2007–2009 La Niña period, show a blocking
846 pattern around Wilkes Land, consistent with transient meridional blocking associated with increased precipitation
847 along the coastline (Udy et al., 2022; Udy et al., 2021). However, given the duration of our defined periods, this
848 transient blocking is likely smoothed out over longer timeframes, which may explain the stronger signal observed
849 during the shorter 2009–2010 El Niño period. The asymmetric shape of the positive pressure anomaly extension
850 off the Wilkes Land is much stronger in the 2009–2010 period, and is consistent with the development of
851 atmospheric blocking in the Tasman Sea region (Pook et al., 2006), which is associated with increased
852 precipitation in Wilkes Land (Pohl et al., 2021; Udy et al., 2022).

853 Our 2020–2022 La Niña period shows significant mass gain across the Indian Ocean and Wilkes Land region and
854 was the only period in our analysis period when La Niña and positive SAM occurred together (Fig. 1c). However,
855 this period also included the March 2022 atmospheric river event, which delivered record-breaking precipitation
856 and heat to East Antarctica (Wille et al., 2024). While this event was not the only atmospheric river to occur
857 during the GRACE period, this four-day event likely had some influence on the mass anomaly patterns of the
858 2020–2022 La Niña period we define in this study. To determine the extent of the influence of this event, we

859 examined the 2020-2022 period by comparing the inclusion and exclusion of the March 2022 event
860 (Supplementary Fig. S5). While the March 2022 event increased the strength of the SMB positive anomaly in
861 Wilkes Land, the region still observed a strong positive SMB anomaly during the 2020-2022 period when March
862 2022 was excluded (Supplementary Fig. S5). According to Wang et al. (2023), extreme events in March 2022 and
863 October 2021 accounted for approximately 38% of the precipitation anomalies in Wilkes Land during the 2020-
864 2022 La Niña period, driven by a pair of symmetrically distributed high-low pressure systems over the Southern
865 Ocean near 120°W and 60°E.

866 **4.3.1 El Niño dominated periods**

867 ~~ENSO impacts West Antarctica through modulation of the ASL via Rossby wave propagation, though the ASL's influence on East Antarctica remains unclear. ENSO induced pressure anomalies in the Pacific Ocean can potentially influence moisture inflow into East Antarctica through the ASL (Li et al., 2022a), as observed during the 2020–2022 La Niña dominated period (Fig. 5a). During El Niño dominated periods, the weakening of the ASL in three out of the four El Niño dominated periods aligns with the formation of a low pressure anomaly in the South Atlantic (Fig. 4a, c–d). This South Atlantic low pressure anomaly, previously associated with El Niño events (Li et al., 2022a), induces equatorward wind flow (cold and dry southerly anomalies), leading to decreased precipitation, reduced SMB and negative mass anomalies in the Atlantic sector of East Antarctica (Fig. 4e, g–h).~~

875 ~~In contrast, the Atlantic sector experienced mass increase during the 2009–2010 El Niño dominated period. The significant mass gain observed in Dronning Maud Land (Atlantic sector) during this period has been attributed to atmospheric blocking, which produced episodic snowfall events (Boening et al., 2012). Atmospheric blocking favours the occurrence of atmospheric rivers reaching the Antarctic coastline and is often associated with increased precipitation and temperature (Wille et al., 2021). The weakening of the westerlies during negative SAM conditions (Clem et al., 2016), allows for Rossby wave amplification and an increased frequency of atmospheric blocking events in East Antarctica, particularly during winter, when the relationship is strongest (Wang et al., 2024). However, no statistically significant relationship has been established between negative SAM and atmospheric river frequency in Dronning Maud Land (Wille et al., 2021). These blocking events significantly impact East Antarctic climate, through their influence on temperatures and precipitation (Wang et al., 2024; Udy et al., 2021; Pohl et al., 2021).~~

886 ~~The 2014–2016 El Niño dominated period demonstrated a spatial pattern in East Antarctica that closely aligned with a positive SAM signal response, resulting in a negative mass anomaly in the region (Fig. 4g). During this period, the strengthened westerlies around 60°S, associated with positive SAM, enhanced moisture transport away from Antarctica, reducing precipitation and leading to the observed negative mass anomaly (Marshall et al., 2017).~~

890 ~~However, differentiating the timescale between individual extreme snowfall events and ice sheet response in monthly GRACE observed ice mass data is complex. Atmospheric rivers, for instance, occur on average less than 5 days per year but can contribute 30–40% of annual precipitation (Wille et al., 2021). Despite the short duration of these events, the impact of ENSO on SMB can be influenced by synoptic scale phenomena, such as atmospheric rivers associated with blocking events (Pohl et al., 2021). These high impact, short term events can disrupt expected ENSO patterns, leading to varied impacts on the ice sheet, as observed in the positive mass anomaly in Dronning Maud Land during the 2009–2010 El Niño dominated period.~~

897 **4.3.2 La Niña dominated periods**

898 ~~La Niña has been linked to high pressure anomaly development in the South Atlantic, which leads to moisture advection into Dronning Maud Land (Li et al., 2022b). This moisture transport results in increased precipitation and a subsequent positive mass anomaly in the region. In two out of the three La Niña dominated periods (2007–2009, 2010–2014 periods) considered, a high pressure anomaly in the South Atlantic is a common feature (Fig. 5a–b).~~

903 Similar to El Niño dominated periods, the response of the East Antarctic Ice sheet during La Niña dominated
904 periods also shows variability, with both consistent and opposing anomaly signals between the Indian and Atlantic
905 sectors. During the 2010–2014 La Niña dominated period, Dronning Maud Land experienced a positive mass
906 anomaly, while Wilkes Land showed a negative mass anomaly (Fig. 5f). By contrast, for the 2020–2022 La Niña-
907 dominated period, both Dronning Maud Land and Wilkes Land exhibited a positive mass anomaly (Fig. 5h),
908 suggesting that, in addition to high pressure anomalies driving moisture into the region, other factors also
909 influence these regional responses.

910 We observed large mass gain during the 2020–2022 La Niña dominated period (Fig. 5h); however, this gain cannot
911 be directly attributed to the amplification of positive SAM and La Niña anomalies, as they appear to be
912 atmospherically in phase (Fig. 1c). Our analysis does not account for the removal of the extreme March 2022
913 heatwave event, which saw record shattering temperature anomalies and widespread snow accumulation (Wille
914 et al., 2024). However, the deepened low pressure anomaly in the Pacific induced strong northerly winds across
915 the Peninsula into Dronning Maud Land, while the symmetric structure of the westerlies was altered, allowing
916 northerly winds to reach Wilkes Land.

917 Ice sheet variability in the Indian sector is influenced by multiple factors and not solely driven by ENSO signals.
918 SAM signals have been found in Wilkes Land (King and Christoffersen, 2024; King et al., 2023), and synoptic
919 weather patterns in the southern Indian Ocean can influence the transport of moisture and heat into the region,
920 ultimately affecting ice mass variability (Udy et al., 2021).

921 Our findings indicate that ice mass changes during ENSO-dominated periods cannot be solely attributed to ENSO
922 forcing. To quantify changes in ENSO variability, long time series must be considered in future studies (Stevenson
923 et al., 2010), along with the use of climate models to better isolate and capture purely ENSO-driven signals.

924 4.4 Combined ENSO and SAM influence

925 Isolating the ENSO signal and its impact on AIS ice mass is challenging due to several factors. The Rossby wave
926 propagation of the ENSO signal to Antarctica is influenced by SAM (Marshall, 2003; Fogt and Marshall, 2020a),
927 and the ENSO signal can be masked by other climate modes, such as zonal-wave 3—a quasi-stationary pattern in
928 the southern high latitudes that affects meridional heat and momentum transport (Goyal et al., 2022; Raphael,
929 2004). Additionally, synoptic-scale weather systems can further mask ENSO’s influence. The complex interaction
930 between ENSO and other modes of climate variability likely drives the equally complex patterns of AIS ice mass
931 change observed during different ENSO-dominated periods.

932 While our analysis does not explicitly resolve the mechanisms through which ENSO and SAM influence wind
933 anomalies, previous studies have demonstrated strong correlations between ENSO and meridional winds, and
934 between SAM and zonal winds, both significantly influencing Antarctic Peninsula climate (Clem et al., 2016).

935 Pressure anomaly variability in the Pacific sector during ENSO-dominated periods can be associated with the
936 cumulative SAM phase. During ENSO periods when the cumulative SAM and ENSO occur in phase (El Niño-/
937 SAM or La Niña/+SAM) (Fogt et al., 2011), the pressure anomaly over the Pacific sector is close to the continent,
938 spatially extensive, and centred around the Amundsen Sea sector (Figs. 4a and 5d). However, during ENSO-

939 dominated periods that are out of phase with the cumulative SAM (El Niño/+SAM or La Niña/-SAM) (Fogt et
940 al., 2011), the pressure anomaly appears northward, away from the continent (Figs. 4c and 5a). Periods where the
941 cumulative SAM phase shows a neutral phase, the pressure anomaly in the Pacific is centred around the
942 Bellingshausen Sea sector (Figs. 4d, 5b, c). However, between 2000 to 2020, shifts in large-scale circulation,
943 particularly in SAM, have been reported, potentially affecting ENSO teleconnections and their influence on AIS
944 variability (Xin et al., 2023).

945 Our analysis, which uses cumulative summed indices to match GRACE mass time series, has limitations. It
946 focuses primarily on low-frequency variability and does not account for shorter temporal scale impacts, such as
947 tropical convection pulses that trigger the Rossby waves or high-frequency variability associated with storm
948 systems such as atmospheric rivers. However, the net effect of these would be captured by GRACE.

949 The combination of La Niña and positive SAM conditions strengthen the ASL (Fogt et al., 2011) and drives
950 positive temperature anomalies across the Antarctic Peninsula and East Antarctica (Clem and Raphael, 2023).
951 This relationship partially explains the significant mass gain observed across these regions during the 2020–2022
952 La Niña dominated periods. The extreme atmospheric river event in March 2022 largely contributed to the
953 observed mass gain over this ENSO dominated period (Wille et al., 2024; Wille et al., 2022).

954 Studies on precipitation (Marshall et al., 2017) and ice core records (Medley and Thomas, 2019) both recognise
955 that SMB generally decreases during positive SAM phase and increases during negative SAM phase. In terms of
956 the impact on basal melting, negative SAM periods generally decrease the transport of warm circumpolar deep
957 water onto the continental shelf (Palóczy et al., 2018), largely reducing ice shelf basal melt (Verfaillie et al., 2022)
958 and subsequently contributing to ice mass gain. However, the timescale of the response of the upstream ice to the
959 positive SAM forcing is unclear and would involve a substantial lag, which can range from months to several
960 years depending on regional ice dynamics (King and Christoffersen, 2024). This suggests that GRACE-derived
961 signals may represent a delayed response rather than an immediate reaction to SAM variability. The spatial pattern
962 of ice mass change anomaly during the 2002–2005 El Niño and 2007–2009 La Niña-dominated periods in the
963 Amundsen Sea sector and Wilkes Land resembles the negative SAM spatial pattern reported by King et al. (2023).
964 Negative SAM dominates the cumulative summed SAM (Fig. 1e) from the start of the GRACE time series in
965 2002 until around 2010, which aligns with the high-positive pressure anomaly observed over Antarctica,
966 reflecting a stronger than average (over the GRACE period) Antarctic high during this period (Figs. 4a–b and
967 5a). Therefore, it is possible that ice mass variability observed between 2002 and 2010 was more influenced by
968 SAM than by ENSO.

969 Our findings agree with an understanding that ENSO forcing on the Antarctic climate impacts
970 atmospheric circulation patterns, altering the ASL variability, which in turn influences Antarctic ice mass
971 variability (Zhang et al., 2021; Paolo et al., 2018; Sasgen et al., 2010; Clem et al., 2017). However, across
972 individual ENSO periods, the AIS response exhibits considerable variability, with each period associated with
973 distinct atmospheric circulation patterns. It is possible that the teleconnection between tropical ENSO signals and
974 Antarctic climate may not be fully established during a given ENSO phase or masked by other processes. Our
975 analysis, which uses cumulative summed indices to match GRACE mass time series, is primarily sensitive to low-

frequency variability and does not resolve shorter-term impacts, such as tropical convection pulses that initiate Rossby wave trains or high-frequency variability linked to storm systems like atmospheric rivers. Nonetheless, the integrated effect of these processes is captured by GRACE. Additionally, The internal dynamics of the ASL may contribute to AIS mass variability that is independent of the influence of ENSO and SAM which potentially can impact our analysis. Given that our analysis spans a 22-year period, long time series must be considered in future studies (Stevenson et al., 2010), along with the use of climate models to better isolate and capture purely ENSO-driven signals. these results primarily capture the interannual variability rather than lower frequency influence of the Pacific Decadal Oscillation signal. While ENSO induced circulation affects Antarctic SMB (Kim et al., 2020), recent Antarctic ice mass trends (2003-2020) have been primarily driven by mass imbalance triggered by long-term ice dynamics changes (Kim et al., 2024; Rignot et al., 2019). Some of the low-frequency mass variability around the long-term trend (which we remove) is associated with changing ice dynamics. This dynamic signal is stronger in West than in East Antarctica (Rignot et al., 2019).

In a warming climate, future ENSO event variability is predicted to increase (Cai et al., 2021). CMIP5 model simulations suggest a reduction in El Niño-induced precipitation over West Antarctica (Lee et al., 2023). Given that SAM is projected to remain in its positive phase across all seasons due to greenhouse gas emissions (Arblaster and Meehl, 2006), accurate modelling of future AIS mass estimates in relation to ENSO teleconnections must account for the interaction between SAM and ENSO. The AIS mass gain observed during 2020-2022 raises questions about how the AIS will respond to future La Niña and positive SAM periods and if it would increase the frequency of extreme events.

5 Conclusion

To examine the AIS mass change during different ENSO-dominated periods, we analysed AIS mass change anomalies observed by GRACE/GRACE-FO spanning the period 2002-2022. These anomalies were interpreted alongside RACMO2.4p1 modelled SMB and atmospheric pressure and wind patterns mean sea level pressure and 10 m winds from ERA5 reanalysis products. Our analysis reveals that El Niño and La Niña periods exert distinct influences on the AIS, with considerable event to event spatial variability.

At the continental scale, three out of the four El Niño-dominated periods were characterised by mass increase in West Antarctica and mass decrease in East Antarctica. Conversely, two out of the three La Niña-dominated periods (here excluding the 2016-2018 period with degraded GRACE signal) showed the opposite pattern, with mass reduction in West Antarctica and to varying degrees, mass increase in East Antarctica. The Amundsen Sea sector typically experiences positive mass anomalies during El Niño-dominated periods and negative anomalies during La Niña-dominated periods. In East Antarctica, a consistent mass increase was observed during two out of three La Niña dominated periods.

Mass variability in West Antarctica is primarily driven by ENSO-induced ASL pressure anomalies, which modulate the atmospheric circulation and moisture transport. The ASL exhibits high variability in its location, strength, and extent, which influence its impact between the Antarctic Peninsula and West Antarctica. The ASL strengthens and moves closer to the Antarctic coastline during periods when ENSO-SAM are in phase (Hosking et al., 2013). While ENSO has its strongest impact in West Antarctica, its influence extends to East Antarctica,

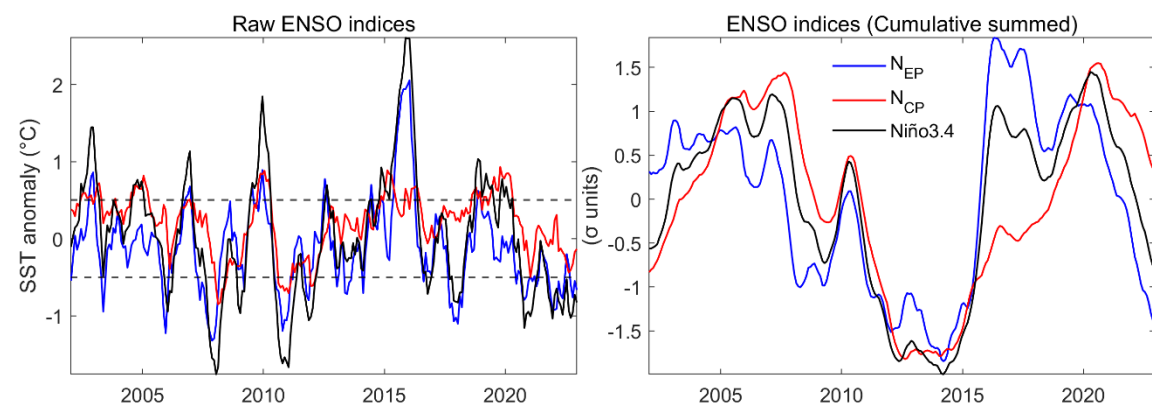
013 ~~consistent with Li et al. (2022a).~~ However, atmospheric pressure patterns over the Southern Ocean play a crucial
014 role in regulating moisture influx and, consequently, ice mass variability in East Antarctica.

1015 In summary, this study highlights the complex nature of ENSO teleconnections in modulating AIS mass balance
1016 through changes in atmospheric circulation. Rather than exhibiting a simple dipole response (Fig. 3), AIS mass
1017 variability during ENSO ~~event~~periods is shaped by unique teleconnections and moisture fluxes specific to each
1018 ~~period~~event. We acknowledge uncertainties in our analysis due to the relatively short ENSO-dominated periods
1019 considered. Some ENSO-related teleconnections may not have fully developed during these intervals, and other
1020 processes—such as atmospheric rivers—may have masked or modulated the ENSO signal, complicating the
1021 attribution of the observed spatial impacts. Although climate model projections remain uncertain regarding
1022 whether future ENSO events will more resemble an El Niño- or La Niña-like state, they consistently indicate that
1023 ENSO will influence Antarctic precipitation patterns. A clearer understanding of ENSO’s role in Antarctic climate
1024 is therefore critical for assessing its impact on future SMB and long-term ice mass balance. This requires both
1025 process-level understanding (e.g., Macha et al., 2024) and consideration of the net effect on ice sheet mass as
1026 explored here.

1027 **Supplementary materials**

1028 **Text S1**

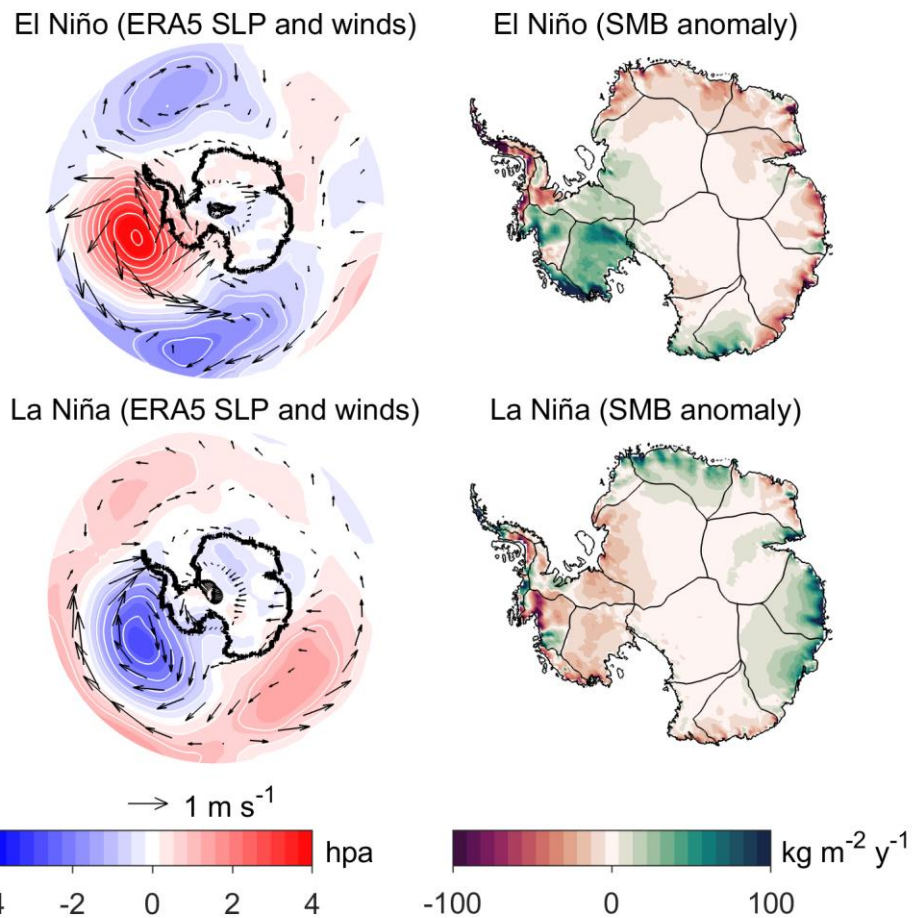
029 Following the method proposed by Ren and Jin (2011), we compute indices for Central and Eastern Pacific ENSO
030 events and compare their normalised and cumulatively summed timeseries to those of the Niño 3.4 index.



032 **Figure S1. Timeseries of various ENSO metric indices.**

033 **Text S2**

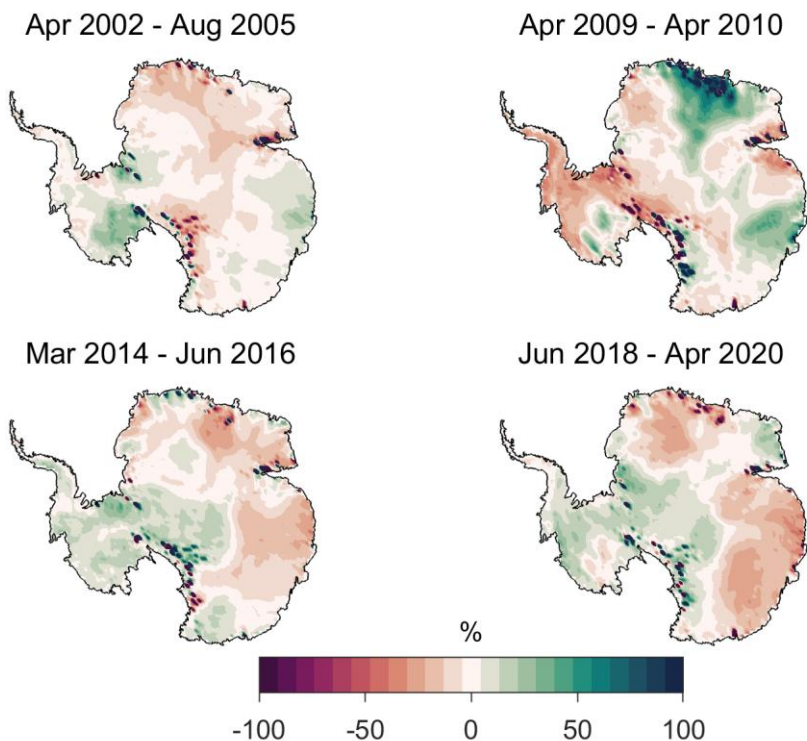
034 Using composite analysis, we examined the spatial patterns of surface mass balance (SMB) and atmospheric
035 anomalies during ENSO years. To achieve this, we first computed annual SMB accumulation anomalies and the
036 annual mean Niño 3.4 index. El Niño and La Niña years were then selected based on threshold values of above
037 0.5 and below -0.5, respectively. Composite maps were subsequently generated for each category. This approach
038 provides an additional framework for comparing our results with those derived from regression analysis.



040
041 **Figure S2. Composite maps showing the impact of El Niño and La Niña events on ERA5 mean sea level**
042 **pressure (shading and contour, hPa) and 10 m wind anomalies (vectors, $m s^{-1}$), alongside surface mass SMB**
043 **anomalies ($kg m^{-2} y^{-1}$) from RACMO2.4p1 over the period 2002-2022.**

044 **Text S3**

045 The relative impact of SMB changes was expressed as a percentage of the climatological mean SMB for each El
046 Niño-dominated period. To achieve this, we computed the mean SMB for each period, compared it to the long-
047 term climatological mean at each grid point, and then expressed the difference as a percentage.



048
049 **Figure S3. Map of RACMO2.4p1 SMB changes, expressed as a percentage relative to the 2002–2022**
050 **climatology during El Niño-dominated periods.**

051 **Text S4**

052 The relative impact of SMB changes was expressed as a percentage of the climatological mean SMB for each La
053 Niña-dominated period. To achieve this, we computed the mean SMB for each period, compared it to the long-
054 term climatological mean at each grid point, and then expressed the difference as a percentage.

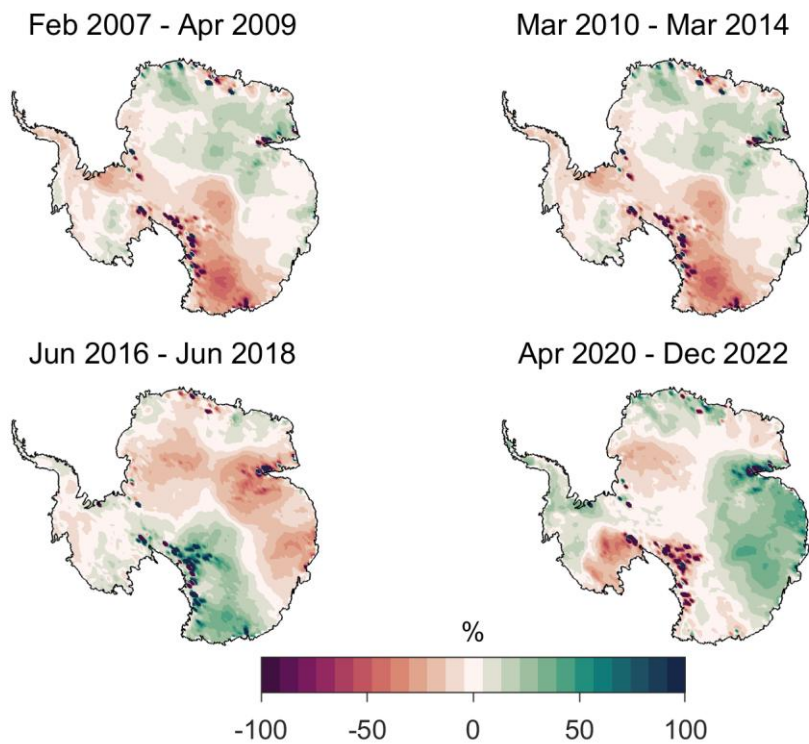
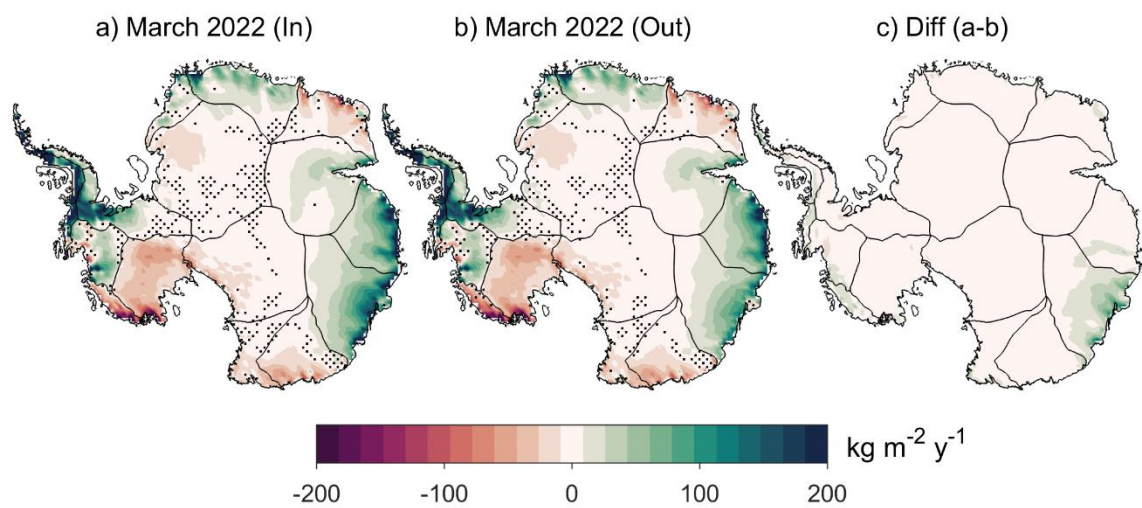


Figure S4. Map of RACMO2.4p1 SMB changes, expressed as a percentage relative to the 2002–2022 climatology during La Niña-dominated periods.

Text S5

The impact of the March 2022 extreme event is assessed by comparing scenarios that include and exclude the event and evaluating the difference between the two.



1063 [Figure S5. Presents maps of SMB anomalies \(kg m⁻² y⁻¹\) during the 2020–2022 La Niña period from](#)
1064 [RACMO2.4p1: \(a\) includes the March 2022 AR event, \(b\) excludes March 2022 AR event, and \(c\) shows](#)
1065 [the difference between \(a\) and \(b\).](#)

1066 **Code and Data availability**

1067 Source code and data will be made available through the University of Tasmania Research Data Portal prior to
1068 publication. The GRACE data used is available at <https://gravis.gfz.de/ais>. The ERA5 reanalysis data used in the
1069 atmospheric linkage to ice mass variation are publicly available from <https://cds.climate.copernicus.eu/>. The
1070 station-derived SAM index from Marshall (2003) available at <http://www.nerc-bas.ac.uk/icd/gjma/sam.html>.
1071 The Niño3.4 index are publicly available from <https://psl.noaa.gov/data/timeseries/month/Nino34/>.
1072 RACMO2.~~43~~^{p21} model SMB output can be accessed at <https://zenodo.org/records/14217232> (Van Dalum et al., 2025; Van Dalum et al., 2024) .-
1073

1074 **Author contributions**

1075 All authors contributed to the conception and design of the study. JBA performed the statistical analysis and data
1076 processing. JBA wrote the manuscript with input from all co-authors. All authors helped with the revision and
1077 approved the final version of the manuscript.

1078 **Competing interests**

1079 The authors declare that they have no conflict of interest.

1080 **Disclaimer**

1081 Publisher's note: Copernicus Publications remains neutral with regard to jurisdictional claims made in the text,
1082 published maps, institutional affiliations, or any other geographical representation in this paper. While Copernicus
1083 Publications makes every effort to include appropriate place names, the final responsibility lies with the authors.

1084 **Acknowledgements**

1085 We thank the GravIS team for supplying GRACE data, the European Centre for Medium-Range Weather
1086 Forecasts for providing reanalysis climatic data, NOAA for the ENSO indices, Marshall (2003) for the SAM index
1087 and [Van Dalum et al. \(2024\)](#)~~finally Van Wessem (2023)~~ for providing the SMB dataset. [Finally, we thank the](#)
1088 [Editor and reviewers for constructive reviews.](#)

1089 **Financial support**

1090 JBA, MK and DU were supported by the Australian Research Council Special Research Initiative, Australian
1091 Centre for Excellence in Antarctic Science (Project Number SR200100008). TV was supported by the Australian
1092 Government's Antarctic Science Collaboration Initiative (ASCI000002) through funding to the Australian
1093 Antarctic Program Partnership. JBA was supported by a University of Tasmania Graduate Research Scholarship.

1094 **References**

1095 Arblaster, J. M. and Meehl, G. A.: Contributions of external forcings to southern annular mode trends, *Journal of*
1096 *Climate*, 19, 2896-2905, Doi 10.1175/Jcli3774.1, 2006.

1097 Baiman, R., Winters, A. C., Lenaerts, J., and Shields, C. A.: Synoptic Drivers of Atmospheric River Induced
1098 Precipitation Near Dronning Maud Land, Antarctica, *Journal of Geophysical Research (Atmospheres)*, 128,
1099 e2022JD037859, 10.1029/2022jd037859, 2023.

1100 Bodart, J. A. and Bingham, R. J.: The Impact of the Extreme 2015-2016 El Nino on the Mass Balance of the
1101 Antarctic Ice Sheet, *Geophysical Research Letters*, 46, 13862-13871, 10.1029/2019gl084466, 2019.

1102 Boening, C., Lebsack, M., Landerer, F., and Stephens, G.: Snowfall-driven mass change on the East Antarctic ice
1103 sheet, *Geophysical Research Letters*, 39, n/a-n/a, Artn L21501
1104 10.1029/2012gl053316, 2012.

1105 Cai, W. J., Santoso, A., Collins, M., Dewitte, B., Karamperidou, C., Kug, J. S., Lengaigne, M., McPhaden, M. J.,
1106 Stuecker, M. F., Taschetto, A. S., Timmermann, A., Wu, L. X., Yeh, S. W., Wang, G. J., Ng, B., Jia, F., Yang,
1107 Y., Ying, J., Zheng, X. T., Bayr, T., Brown, J. R., Capotondi, A., Cobb, K. M., Gan, B. L., Geng, T., Ham, Y. G.,
1108 Jin, F. F., Jo, H. S., Li, X. C., Lin, X. P., McGregor, S., Park, J. H., Stein, K., Yang, K., Zhang, L., and Zhong,
1109 W. X.: Changing El Nino-Southern Oscillation in a warming climate, *Nature Reviews Earth & Environment*, 2,
1110 628-644, 10.1038/s43017-021-00199-z, 2021.

1111 Chen, X. Y., Li, S. L., and Zhang, C.: Distinct impacts of two kinds of El Nino on precipitation over the Antarctic
1112 Peninsula and West Antarctica in austral spring, *Atmospheric and Oceanic Science Letters*, 16, 100387, ARTN
1113 100387
1114 10.1016/j.aosl.2023.100387, 2023.

1115 Clem, K. R. and Fogt, R. L.: Varying roles of ENSO and SAM on the Antarctic Peninsula climate in austral spring,
1116 *J Geophys Res-Atmos*, 118, 11481-11492, 10.1002/jgrd.50860, 2013.

1117 Clem, K. R. and Raphael, M. N.: Antarctica and the Southern Ocean, *Bulletin of the American Meteorological
1118 Society*, 104, S322-S365, 10.1175/Bams-D-23-0077.1, 2023.

1119 Clem, K. R., Renwick, J. A., and McGregor, J.: Large-Scale Forcing of the Amundsen Sea Low and Its Influence
1120 on Sea Ice and West Antarctic Temperature, *Journal of Climate*, 30, 8405-8424, 10.1175/Jcli-D-16-0891.1, 2017.

1121 Clem, K. R., Renwick, J. A., McGregor, J., and Fogt, R. L.: The relative influence of ENSO and SAM on Antarctic
1122 Peninsula climate, *J Geophys Res-Atmos*, 121, 9324-9341, 10.1002/2016jd025305, 2016.

1123 Dahle, C., Murböck, M., Flechtner, F., Dobslaw, H., Michalak, G., Neumayer, K. H., Abrykosov, O., Reinhold,
1124 A., König, R., Sulzbach, R., and Förste, C.: The GFZ GRACE RL06 Monthly Gravity Field Time Series:
1125 Processing Details and Quality Assessment, *Remote Sensing*, 11, 2116, ARTN 2116
1126 10.3390/rs11182116, 2019.

1127 Dahle, C., Boergens, E., Sasgen, I., Döhne, T., Reißland, S., Dobslaw, H., Kleemann, V., Murböck, M., König, R.,
1128 Dill, R., Sips, M., Sylla, U., Groh, A., Horwath, M., and Flechtner, F.: GravIS: mass anomaly products from
1129 satellite gravimetry, 10.5194/essd-2024-347, 2024.

1130 Diener, T., Sasgen, I., Agosta, C., Fuerst, J. J., Braun, M. H., Konrad, H., and Fettweis, X.: Acceleration of
1131 Dynamic Ice Loss in Antarctica From Satellite Gravimetry, *Frontiers in Earth Science*, 9, ARTN 741789
1132 10.3389/feart.2021.741789, 2021.

1133 Fogt, R. L. and Marshall, G. J.: The Southern Annular Mode: Variability, trends, and climate impacts across the
1134 Southern Hemisphere, *Wiley Interdisciplinary Reviews-Climate Change*, 11, ARTN e652
1135 10.1002/wcc.652, 2020a.

1136 Fogt, R. L. and Marshall, G. J.: The Southern Annular Mode: Variability, trends, and climate impacts across the
1137 Southern Hemisphere, *WIREs Climate Change*, 11, 10.1002/wcc.652, 2020b.

1138 Fogt, R. L., Bromwich, D. H., and Hines, K. M.: Understanding the SAM influence on the South Pacific ENSO
1139 teleconnection, *Climate Dyn.*, 36, 1555-1576, 2011.

1140 Fogt, R. L., Jones, J. M., and Renwick, J.: Seasonal Zonal Asymmetries in the Southern Annular Mode and Their
1141 Impact on Regional Temperature Anomalies, *Journal of Climate*, 25, 6253-6270, 10.1175/jcli-d-11-00474.1,
1142 2012.

1143 Gardner, A. S., Moholdt, G., Scambos, T., Fahnestock, M., Ligtenberg, S., van den Broeke, M., and Nilsson, J.:
1144 Increased West Antarctic and unchanged East Antarctic ice discharge over the last 7 years, *Cryosphere*, 12, 521-
1145 547, 10.5194/tc-12-521-2018, 2018.

1146 Goyal, R., Jucker, M., Gupta, A. S., and England, M. H.: A New Zonal Wave-3 Index for the Southern
1147 Hemisphere, *Journal of Climate*, 35, 5137-5149, 10.1175/Jcli-D-21-0927.1, 2022.

1148 Groh, A. and Horwath, M.: The method of tailored sensitivity kernels for GRACE mass change estimates, April
1149 01, 20162016.

1150 Hersbach, H., Bell, B., Berrisford, P., Hirahara, S., Horányi, A., Muñoz-Sabater, J., Nicolas, J., Peubey, C., Radu,
1151 R., Schepers, D., Simmons, A., Soci, C., Abdalla, S., Abellán, X., Balsamo, G., Bechtold, P., Biavati, G., Bidlot,
1152 J., Bonavita, M., De Chiara, G., Dahlgren, P., Dee, D., Diamantakis, M., Dragani, R., Flemming, J., Forbes, R.,

1153 Fuentes, M., Geer, A., Haimberger, L., Healy, S., Hogan, R. J., Hólm, E., Janisková, M., Keeley, S., Laloyaux, P., Lopez, P., Lupu, C., Radnoti, G., de Rosnay, P., Rozum, I., Vamborg, F., Villaume, S., and Thépaut, J. N.:
 1154 The ERA5 global reanalysis, *Quarterly Journal of the Royal Meteorological Society*, 146, 1999-2049,
 1155 10.1002/qj.3803, 2020.

1156 Hosking, J. S., Orr, A., Marshall, G. J., Turner, J., and Phillips, T.: The Influence of the Amundsen-Bellingshausen
 1157 Seas Low on the Climate of West Antarctica and Its Representation in Coupled Climate Model Simulations,
 1158 *Journal of Climate*, 26, 6633-6648, 10.1175/Jcli-D-12-00813.1, 2013.

1159 Hoskins, B. J. and Karoly, D. J.: The Steady Linear Response of a Spherical Atmosphere to Thermal and
 1160 Orographic Forcing, *Journal of the Atmospheric Sciences*, 38, 1179-1196, Doi 10.1175/1520-
 1161 0469(1981)038<1179:Tslroa>2.0.Co;2, 1981.

1162 Huguenin, M. F., Holmes, R. M., Spence, P., and England, M. H.: Subsurface Warming of the West Antarctic
 1163 Continental Shelf Linked to El Niño-Southern Oscillation, *Geophysical Research Letters*, 51, ARTN
 1164 e2023GL104518
 1165 10.1029/2023GL104518, 2024.

1166 Kim, B. H., Seo, K. W., Eom, J., Chen, J., and Wilson, C. R.: Antarctic ice mass variations from 1979 to 2017
 1167 driven by anomalous precipitation accumulation, *Sci Rep*, 10, 20366, 10.1038/s41598-020-77403-5, 2020.

1168 Kim, B. H., Seo, K. W., Lee, C. K., Kim, J. S., Lee, W. S., Jin, E. K., and van den Broeke, M.: Partitioning the
 1169 drivers of Antarctic glacier mass balance (2003-2020) using satellite observations and a regional climate model,
 1170 *Proc Natl Acad Sci U S A*, 121, e2322622121, 10.1073/pnas.2322622121, 2024.

1171 Kim, J., Kim, W., Yeh, S., KUG, J., and Kwon, M.: The unique 2009-2010 El Niño event: A fast phase transition
 1172 of warm pool El Niño to La Niña, *AGU Fall Meeting Abstracts*, December 01, 20112011.

1173 King, M. A. and Christoffersen, P.: Major Modes of Climate Variability Dominate Nonlinear Antarctic Ice-Sheet
 1174 Elevation Changes 2002-2020, *Geophysical Research Letters*, 51, ARTN e2024GL108844
 1175 10.1029/2024GL108844, 2024.

1176 King, M. A., Lyu, K., and Zhang, X. B.: Climate variability a key driver of recent Antarctic ice-mass change,
 1177 *Nature Geoscience*, 16, 1128-1135, 10.1038/s41561-023-01317-w, 2023.

1178 Landerer, F. W., Flechtner, F. M., Save, H., Webb, F. H., Bandikova, T., Bertiger, W. I., Bettadpur, S. V., Byun,
 1179 S. H., Dahle, C., Dobslaw, H., Fahnestock, E., Harvey, N., Kang, Z. G., Kruizinga, G. L. H., Loomis, B. D.,
 1180 McCullough, C., Murböck, M., Nagel, P., Paik, M., Pie, N., Poole, S., Strekalov, D., Tamisiea, M. E., Wang, F.
 1181 R., Watkins, M. M., Wen, H. Y., Wiese, D. N., and Yuan, D. N.: Extending the Global Mass Change Data Record:
 1182 GRACE Follow-On Instrument and Science Data Performance, *Geophysical Research Letters*, 47, ARTN
 1183 e2020GL088306
 1184 10.1029/2020GL088306, 2020.

1185 Lee, H.-J., Jin, E. K., Kim, B.-H., and Lee, W. S.: Vanishing of the El Niño-induced delay effect on the ice mass
 1186 loss of West Antarctica in future climate change, 10.21203/rs.3.rs-2437498/v1, 2023.

1187 Li, Z., Chao, B. F., Wang, H., and Zhang, Z.: Antarctica ice-mass variations on interannual timescale: Coastal
 1188 Dipole and propagating transports, *Earth and Planetary Science Letters*, 595, 117789, ARTN 117789
 1189 10.1016/j.epsl.2022.117789, 2022a.

1190 Li, Z., Chao, B. F., Wang, H. S., and Zhang, Z. Z.: Antarctica ice-mass variations on interannual timescale: Coastal
 1191 Dipole and propagating transports, *Earth Plan. Sci. Lett.*, 595, 117789,
 1192 <https://doi.org/10.1016/j.epsl.2022.117789>, 2022b.

1193 Macha, J. M. A., Mackintosh, A. N., McCormack, F. S., Henley, B. J., McGregor, H. V., van Dalum, C. T., and
 1194 Purich, A.: Distinct Central and Eastern Pacific El Niño Influence on Antarctic Surface Mass Balance,
 1195 *Geophysical Research Letters*, 51, ARTN e2024GL109423
 1196 10.1029/2024GL109423, 2024.

1197 Marshall, G. J.: Trends in the southern annular mode from observations and reanalyses, *Journal of Climate*, 16,
 1198 4134-4143, Doi 10.1175/1520-0442(2003)016<4134:TitSam>2.0.Co;2, 2003.

1199 Marshall, G. J., Orr, A., and Turner, J.: A Predominant Reversal in the Relationship between the SAM and East
 1200 Antarctic Temperatures during the Twenty-First Century, *Journal of Climate*, 26, 5196-5204, 10.1175/Jcli-D-12-
 1201 00671.1, 2013.

1202 Marshall, G. J., Thompson, D. W. J., and van den Broeke, M. R.: The Signature of Southern Hemisphere
 1203 Atmospheric Circulation Patterns in Antarctic Precipitation, *Geophys Res Lett*, 44, 11580-11589,
 1204 10.1002/2017GL075998, 2017.

1205 McPhaden, M. J., Zebiak, S. E., and Glantz, M. H.: ENSO as an integrating concept in earth science, *Science*,
 1206 314, 1740-1745, 10.1126/science.1132588, 2006.

1207 Medley, B. and Thomas, E. R.: Increased snowfall over the Antarctic Ice Sheet mitigated twentieth-century sea-
 1208 level rise, *Nature Climate Change*, 9, 34-+, 10.1038/s41558-018-0356-x, 2019.

1209 Orr, A., Marshall, G. J., Hunt, J. C. R., Sommeria, J., Wang, C.-G., Van Lipzig, N. P. M., Cresswell, D., and King,
 1210 J. C.: Characteristics of Summer Airflow over the Antarctic Peninsula in Response to Recent Strengthening of

1212 Westerly Circumpolar Winds, *Journal of the Atmospheric Sciences*, 65, 1396-1413, 10.1175/2007jas2498.1, 1213 2008.

1214 Palócz, A., Gille, S. T., and McClean, J. L.: Oceanic Heat Delivery to the Antarctic Continental Shelf: Large- 1215 Scale, Low-Frequency Variability, *Journal of Geophysical Research: Oceans*, 123, 7678-7701, 1216 10.1029/2018jc014345, 2018.

1217 Paolo, F. S., Padman, L., Fricker, H. A., Adusumilli, S., Howard, S., and Siegfried, M. R.: Response of Pacific- 1218 sector Antarctic ice shelves to the El Niño/Southern Oscillation, *Nat Geosci*, 11, 121-126, 10.1038/s41561-017- 1219 0033-0, 2018.

1220 Pohl, B., Favier, V., Wille, J., Udy, D. G., Vance, T. R., Pergaud, J., Dutrievoz, N., Blanchet, J., Kittel, C., Amory, 1221 C., Krinner, G., and Codron, F.: Relationship Between Weather Regimes and Atmospheric Rivers in East 1222 Antarctica, *Journal of Geophysical Research: Atmospheres*, 126, 10.1029/2021jd035294, 2021.

1223 Pook, M. J., McIntosh, P. C., and Meyers, G. A.: The Synoptic Decomposition of Cool-Season Rainfall in the 1224 Southeastern Australian Cropping Region, *Journal of Applied Meteorology and Climatology*, 45, 1156-1170, 1225 10.1175/jam2394.1, 2006.

1226 Raphael, M. N.: A zonal wave 3 index for the Southern Hemisphere, *Geophysical Research Letters*, 31, n/a-n/a, 1227 Artn L23212 10.1029/2004gl020365, 2004.

1228 Raphael, M. N., Marshall, G. J., Turner, J., Fogt, R. L., Schneider, D., Dixon, D. A., Hosking, J. S., Jones, J. M., 1229 and Hobbs, W. R.: THE AMUNDSEN SEA LOW Variability, Change, and Impact on Antarctic Climate, *Bulletin of the American Meteorological Society*, 97, 111-121, 10.1175/Bams-D-14-00018.1, 2016a.

1230 Raphael, M. N., Marshall, G. J., Turner, J., Fogt, R. L., Schneider, D., Dixon, D. A., Hosking, J. S., Jones, J. M., 1231 and Hobbs, W. R.: The Amundsen Sea Low: Variability, Change, and Impact on Antarctic Climate, *Bulletin of the American Meteorological Society*, 97, 111-121, 10.1175/bams-d-14-00018.1, 2016b.

1232 Rayner, N. A., Parker, D. E., Horton, E. B., Folland, C. K., Alexander, L. V., Rowell, D. P., Kent, E. C., and 1233 Kaplan, A.: Global analyses of sea surface temperature, sea ice, and night marine air temperature since the late 1234 nineteenth century, *J Geophys Res-Atmos*, 108, Artn 4407 10.1029/2002jd002670, 2003.

1235 Ren, H. L. and Jin, F. F.: Nino indices for two types of ENSO, *Geophysical Research Letters*, 38, n/a-n/a, Artn 1236 L04704 10.1029/2010gl046031, 2011.

1237 Richard Peltier, W., Argus, D. F., and Drummond, R.: Comment on “An Assessment of the ICE-6G_C (VM5a) 1238 Glacial Isostatic Adjustment Model” by Purcell et al, *Journal of Geophysical Research: Solid Earth*, 123, 2019- 1239 2028, 10.1002/2016jb013844, 2018.

1240 Rignot, E., Mouginot, J., Scheuchl, B., van den Broeke, M., van Wessem, M. J., and Morlighem, M.: Four decades 1241 of Antarctic Ice Sheet mass balance from 1979-2017, *Proc Natl Acad Sci U S A*, 116, 1095-1103, 1242 10.1073/pnas.1812883116, 2019.

1243 Sasgen, I., Groh, A., and Horwath, M.: COST-G GravIS RL01 ice-mass change products, 2020.

1244 Sasgen, I., Dobslaw, H., Martinec, Z., and Thomas, M.: Satellite gravimetry observation of Antarctic snow 1245 accumulation related to ENSO, *Earth and Planetary Science Letters*, 299, 352-358, 10.1016/j.epsl.2010.09.015, 1246 2010.

1247 Scarchilli, C., Frezzotti, M., and Ruti, P. M.: Snow precipitation at four ice core sites in East Antarctica: 1248 provenance, seasonality and blocking factors, *Climate Dynamics*, 37, 2107-2125, 10.1007/s00382-010-0946-4, 1249 2011.

1250 Schneider, D. P., Okumura, Y., and Deser, C.: Observed Antarctic Interannual Climate Variability and Tropical 1251 Linkages, *Journal of Climate*, 25, 4048-4066, 10.1175/Jcli-D-11-00273.1, 2012.

1252 Shepherd, A., Ivins, E. R., A, G., Barletta, V. R., Bentley, M. J., Bettadpur, S., Briggs, K. H., Bromwich, D. H., 1253 Forsberg, R., Galin, N., Horwath, M., Jacobs, S., Joughin, I., King, M. A., Lenaerts, J. T., Li, J., Ligtenberg, S. 1254 R., Luckman, A., Luthcke, S. B., McMillan, M., Meister, R., Milne, G., Mouginot, J., Muir, A., Nicolas, J. P., 1255 Paden, J., Payne, A. J., Pritchard, H., Rignot, E., Rott, H., Sorenson, L. S., Scambos, T. A., Scheuchl, B., Schrama, 1256 E. J., Smith, B., Sundal, A. V., van Angelen, J. H., van de Berg, W. J., van den Broeke, M. R., Vaughan, D. G., 1257 Velicogna, I., Wahr, J., Whitehouse, P. L., Wingham, D. J., Yi, D., Young, D., and Zwally, H. J.: A reconciled 1258 estimate of ice-sheet mass balance, *Science*, 338, 1183-1189, 10.1126/science.1228102, 2012.

1259 Shields, C. A., Wille, J. D., Marquardt Collow, A. B., MacLennan, M., and Gorodetskaya, I. V.: Evaluating 1260 Uncertainty and Modes of Variability for Antarctic Atmospheric Rivers, *Geophysical Research Letters*, 49, 1261 10.1029/2022gl099577, 2022.

1262 Stevenson, S., Fox-Kemper, B., Jochum, M., Rajagopalan, B., and Yeager, S. G.: ENSO Model Validation Using 1263 Wavelet Probability Analysis, *Journal of Climate*, 23, 5540-5547, 10.1175/2010jcli3609.1, 2010.

1264 Swenson, S., Chambers, D., and Wahr, J.: Estimating geocenter variations from a combination of GRACE and 1265 ocean model output, *Journal of Geophysical Research-Solid Earth*, 113, Artn B08410 10.1029/2007jb005338, 2008.

1272 Tapley, B. D., Bettadpur, S., Ries, J. C., Thompson, P. F., and Watkins, M. M.: GRACE measurements of mass
1273 variability in the Earth system, *Science*, 305, 503-505, 10.1126/science.1099192, 2004.

1274 team, I.: Mass balance of the Antarctic Ice Sheet from 1992 to 2017, *Nature*, 558, 219-222, 10.1038/s41586-018-
1275 0179-y, 2018.

1276 Turner, J.: The El Nino-southern oscillation and Antarctica, *International Journal of Climatology*, 24, 1-31,
1277 10.1002/joc.965, 2004.

1278 Turner, J., Phillips, T., Hosking, J. S., Marshall, G. J., and Orr, A.: The Amundsen Sea low, *International Journal*
1279 *of Climatology*, 33, 1818-1829, 10.1002/joc.3558, 2012.

1280 Turner, J., Orr, A., Gudmundsson, G. H., Jenkins, A., Bingham, R. G., Hillenbrand, C. D., and Bracegirdle, T. J.:
1281 Atmosphere-ocean-ice interactions in the Amundsen Sea Embayment, West Antarctica, *Reviews of Geophysics*,
1282 55, 235-276, 10.1002/2016rg000532, 2017.

1283 Udy, D. G., Vance, T. R., Kiem, A. S., and Holbrook, N. J.: A synoptic bridge linking sea salt aerosol
1284 concentrations in East Antarctic snowfall to Australian rainfall, *Communications Earth & Environment*, 3, ARTN
1285 175
1286 10.1038/s43247-022-00502-w, 2022.

1287 Udy, D. G., Vance, T. R., Kiem, A. S., Holbrook, N. J., and Curran, M. A. J.: Links between Large Scale Modes
1288 of Climate Variability and Synoptic Weather Patterns in the Southern Indian Ocean, *Journal of Climate*, 34, 883-
1289 899, 10.1175/Jcli-D-20-0297.1, 2021.

1290 van Dalum, C., Van de Berg, W., and van den Broeke, M.: RACMO2. 3p3 monthly SMB, SEB and t2m data for
1291 Antarctica (1979–2018), Zenodo [data set], 2021.

1292 van Dalum, C. T., van de Berg, W. J., van den Broeke, M. R., and van Tiggelen, M.: The surface mass balance
1293 and near-surface climate of the Antarctic ice sheet in RACMO2.4p1, EGUSphere, 2025, 1-40, 10.5194/egusphere-
1294 2024-3728, 2025.

1295 Van Dalum, C. T., Van De Berg, W. J., Gadde, S. N., Van Tiggelen, M., Van Der Drift, T., Van Meijgaard, E.,
1296 Van Ulft, L. H., and Van Den Broeke, M. R.: First results of the polar regional climate model RACMO2.4, *The*
1297 *Cryosphere*, 18, 4065-4088, 10.5194/tc-18-4065-2024, 2024.

1298 van de Berg, W. J., van den Broeke, M. R., Reijmer, C. H., and van Meijgaard, E.: Reassessment of the Antarctic
1299 surface mass balance using calibrated output of a regional atmospheric climate model, *Journal of Geophysical*
1300 *Research: Atmospheres*, 111, 10.1029/2005jd006495, 2006.

1301 Van Wessem, J. M.: Data set: Monthly averaged RACMO2.3p2 variables; Antarctica, Zenodo [dataset], 2023.

1302 Verfaillie, D., Pelletier, C., Goosse, H., Jourdain, N. C., Bull, C. Y. S., Dalaïden, Q., Favier, V., Fichefet, T., and
1303 Wille, J. D.: The circum-Antarctic ice-shelves respond to a more positive Southern Annular Mode with regionally
1304 varied melting, *Communications Earth & Environment*, 3, 139, ARTN 139
1305 10.1038/s43247-022-00458-x, 2022.

1306 Wang, S.: New record of explosive warmings in East Antarctica, *Sci. Bull.*, 68, 129-132, 2023.

1307 Wang, S., Ding, M. H., Liu, G., Li, G. C., and Chen, W.: Blocking Events in East Antarctica: Impact on
1308 Precipitation and their Association with Large-Scale Atmospheric Circulation Modes, *Journal of Climate*, 37,
1309 1333-1345, 10.1175/Jcli-D-23-0419.1, 2024.

1310 Wang, W., Shen, Y. Z., Chen, Q. J., and Wang, F. W.: Unprecedented mass gain over the Antarctic ice sheet
1311 between 2021 and 2022 caused by large precipitation anomalies, *Environmental Research Letters*, 18, 124012,
1312 ARTN 124012
1313 10.1088/1748-9326/ad0863, 2023.

1314 Wille, J. D., Favier, V., Gorodetskaya, I. V., Agosta, C., Kittel, C., Beeman, J. C., Jourdain, N. C., Lenaerts, J. T.
1315 M., and Codron, F.: Antarctic Atmospheric River Climatology and Precipitation Impacts, *J Geophys Res-Atmos*,
1316 126, ARTN e2020JD033788
1317 10.1029/2020JD033788, 2021.

1318 Wille, J. D., Favier, V., Jourdain, N. C., Kittel, C., Turton, J. V., Agosta, C., Gorodetskaya, I. V., Picard, G.,
1319 Codron, F., Leroy-Dos Santos, C., Amory, C., Fettweis, X., Blanchet, J., Jomelli, V., and Berchet, A.: Intense
1320 atmospheric rivers can weaken ice shelf stability at the Antarctic Peninsula, *Communications Earth &*
1321 *Environment*, 3, ARTN 90
1322 10.1038/s43247-022-00422-9, 2022.

1323 Wille, J. D., Alexander, S. P., Amory, C., Baiman, R., Barthélémy, L., Bergstrom, D. M., Berne, A., Binder, H.,
1324 Blanchet, J., Bozkurt, D., Bracegirdle, T. J., Casado, M., Choi, T., Clem, K. R., Codron, F., Datta, R., Di Battista,
1325 S., Favier, V., Francis, D., Fraser, A. D., Fourré, E., Garreaud, R. D., Genton, C., Gorodetskaya, I., González-
1326 Herrero, S., Heinrich, V. J., Hubert, G., Joos, H., Kim, S. J., King, J. C., Kittel, C., Landais, A., Lazzara, M.,
1327 Leonard, G. H., Lieser, J. L., MacLennan, M., Mikolajczyk, D., Neff, P., Ollivier, I., Picard, G., Pohl, B., Ralph,
1328 F. M., Rowe, P., Schlosser, E., Shields, C. A., Smith, I. J., Sprenger, M., Trusel, L., Udy, D., Vance, T., Walker,
1329 C., Wever, N., and Zou, X.: The Extraordinary March 2022 East Antarctica "Heat" Wave. Part I: Observations
1330 and Meteorological Drivers, *Journal of Climate*, 37, 757-778, 10.1175/Jcli-D-23-0175.1, 2024.

1331 Williams, S. D. P., Moore, P., King, M. A., and Whitehouse, P. L.: Revisiting GRACE Antarctic ice mass trends
1332 and accelerations considering autocorrelation, *Earth and Planetary Science Letters*, 385, 12-21,
1333 <https://doi.org/10.1016/j.epsl.2013.10.016>, 2014.

1334 Xin, M., Clem, K. R., Turner, J., Stammerjohn, S. E., Zhu, J., Cai, W., and Li, X.: West-warming East-cooling
1335 trend over Antarctica reversed since early 21st century driven by large-scale circulation variation, *Environmental
1336 Research Letters*, 18, 064034, 10.1088/1748-9326/acd8d4, 2023.

1337 Zhan, J. G., Shi, H. L., Wang, Y., and Yao, Y. X.: Complex Principal Component Analysis of Antarctic Ice Sheet
1338 Mass Balance, *Remote Sensing*, 13, 480, ARTN 480
1339 10.3390/rs13030480, 2021.

1340 Zhang, B., Yao, Y. B., Liu, L., and Yang, Y. J.: Interannual ice mass variations over the Antarctic ice sheet from
1341 2003 to 2017 were linked to El Nino-Southern Oscillation, *Earth and Planetary Science Letters*, 560, 116796,
1342 ARTN 116796
1343 10.1016/j.epsl.2021.116796, 2021.

1344